

Journal Pre-proofs

Double diffusion in a rectangular duct using metals or oxides suspended in a viscous fluid

J.C. Umavathi, Bernardo Buonomo, Oronzio Manca, Mikhail Sheremet

PII: S2451-9049(20)30313-9
DOI: <https://doi.org/10.1016/j.tsep.2020.100793>
Reference: TSEP 100793

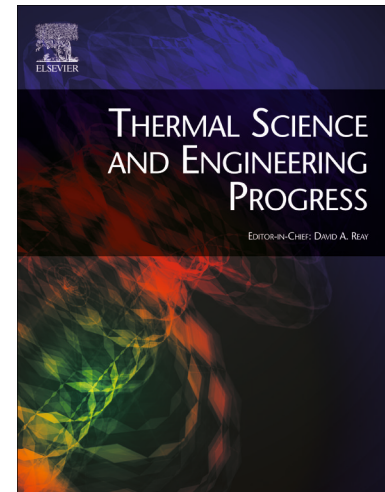
To appear in: *Thermal Science and Engineering Progress*

Received Date: 6 June 2020
Revised Date: 19 November 2020
Accepted Date: 19 November 2020

Please cite this article as: J.C. Umavathi, B. Buonomo, O. Manca, M. Sheremet, Double diffusion in a rectangular duct using metals or oxides suspended in a viscous fluid, *Thermal Science and Engineering Progress* (2020), doi: <https://doi.org/10.1016/j.tsep.2020.100793>

This is a PDF file of an article that has undergone enhancements after acceptance, such as the addition of a cover page and metadata, and formatting for readability, but it is not yet the definitive version of record. This version will undergo additional copyediting, typesetting and review before it is published in its final form, but we are providing this version to give early visibility of the article. Please note that, during the production process, errors may be discovered which could affect the content, and all legal disclaimers that apply to the journal pertain.

© 2020 Published by Elsevier Ltd.



Double diffusion in a rectangular duct using metals or oxides suspended in a viscous fluid

J.C. Umavathi¹, Bernardo Buonomo², Oronzio Manca², Mikhail Sheremet³

¹Department of Mathematics, Gulbarga University, Gulbarga-585 106, Karnataka, India

²Dipartimento di Ingegneria, Univeristà degli Studi della Campania “Luigi Vanvitelli”, Via Roma 29, 81031, Aversa (CE) Italy

³Laboratory on Convective Heat and Mass Transfer, Tomsk State University, 36 Lenin Avenue, 634050 Tomsk, Russia

Abstract

In this study, double diffusive free convection of nanofluid within a confined rectangular duct is investigated numerically. The momentum and energy equations are placed in the form of difference equations and solved numerically. The left wall conditions for the concentration and temperature are lesser than those of the right wall and the upper and lower walls are insulated. Different nanofluids are considered such as mixtures with copper, diamond, silicon oxide and titanium oxide, suspended in water. Brinkman and Maxwell models are used to characterize the nanofluid. Tiwari and Das model is opted to define the nanofluid behavior. The simulations are conducted using different nanoparticles, thermal Grashof number $1 \leq Gr_T \leq 20$, solute Grashof number $1 \leq Gr_C \leq 15$, solid volume fraction $0 \leq \Phi \leq 0.05$, Dufour number $0 \leq Df \leq 1$, Brinkman number $0 \leq Br \leq 2$, and Soret number $0 \leq Sr \leq 5$. Additionally, behavior of volumetric flow strength, skin friction, heat transport intensity and Sherwood number is also examined. The thermal Grashof number, Brinkman number, Dufour, Soret and Schmidt parameters accelerate the velocity and temperature and dwindle the concentration whereas the reversal effect was obtained for the solid volume fraction. The concentration Grashof number diminishes the velocity and temperature and intensifies the concentration. The silver nanoparticles produce the utmost velocity whereas diamond nanoparticles cause the lowest velocity and temperature. The maximum temperature is attained with silicon oxide.

Key words: Viscous fluid, nanoparticles, single-phase nanofluid model, rectangular duct, double diffusion

Nomenclature

A	length to width ratio (a/b)
a	length of the duct [m]
b	breadth of the duct [m]
Br	Brinkman number
C	dimensional concentration
c	concentration in dimensionless form
C_s	concentration susceptibility [kg/J]
C_p	specific heat at constant pressure [$J/(kg \cdot K)$]
D	solotal diffusivity [m^2/s]
D_f	Dufour parameter $\left(\left(\frac{D}{\nu} \right)_f \frac{K_{Tf} (C_2 - C_1)}{C_s C_p (T_2 - T_1)} \right)$
g	gravitational acceleration [m/s^2]
GrT	thermal Grashof number $(g \beta_T \Delta T b^3 \rho_f^2 / \mu_f^2)$
GrC	solute Grashof number $(g \beta_C \Delta C b^3 \rho_f^2 / \mu_f^2)$
K	conductivity of the fluid [$W/(mK)$]
K_{Tf}	thermal diffusion ratio
P	pressure [Pa]
Pr	Prandtl number $(\nu/\alpha)_f$
Q	volumetric flow rate
Sc	Schmidt number $(\nu/D)_f$
Sr	Soret number $\left(\left(\frac{D}{\nu} \right)_f \frac{K_{Tf} (T_2 - T_1)}{T_m (C_2 - C_1)} \right)$
T	temperature [K]
T_0	reference temperature [K]
U, V, W	components of velocity [m/s]
u, v, w	velocity components without dimension
X, Y, Z	coordinates of space [m]
x, y, z	dimensionless space coordinates

Greek symbols

α	heat diffusivity [m^2/s]
β_C	volumetric solutal expansion coefficient
β_T	parameter of heat expansion [K^{-1}]
ρ	density [kg/m^3]
μ	dynamic viscosity [$Pa \cdot s$]
ν	kinematic viscosity [m^2/s]
Φ	solid volume fraction
θ	dimensionless temperature

Subscripts

1	left wall
2	right wall
f	base fluid
m	mean
nf	nanofluid
s	solid particles

1. Introduction

Studies on nanofluid filled system are rapidly increasing because of obscurity in this field. In convection problems the complexity increases for double-diffusion process. Diffusion of moistures in fibrous insulation, drying, electro chemical processes, movement of contaminants or pollutants in soil or air require the examination adopting double-diffusion convection. So, the researchers are interested to think on properties of energy and mass transport in chambers. Nuclear reactors, geothermal reservoirs, heat exchangers, crystal growth in liquids, electronic cooling and chemical processing equipments are some of the areas of applications of double diffusions.

Manca et al. [1] reviewed computationally mixed convection within an open basin bounded by a horizontally insulated plate for different flows. They concluded that opposing forced motion causes the optimal mean Nusselt number. Reviews on the analysis of moisture and energy transfer in conduits were performed by Wee et al. [2] and Beghein et al. [3]. Ghorayeb et al. [4] analyzed conditions for the origin of oscillatory flow numerically in a square chamber. They showed the consequence of Lewis parameter on the transition between steady and oscillatory modes. Adopting adiabatic conditions on the

horizontal plates and flux conditions on the vertical plates, Mamou et al. [5] discussed the free convection over the rectangular vessel. The analysis using non-Darcy model was surveyed by Trevisan and Bejan [6] on the binary diffusion in a square cell. Goyeau et al. [7] and Bennacer et al. [8] also researched for the same geometry for diffusions.

Water, oils, ethylene glycol and other conventional heat transfer fluids have low energy transfer because they have low thermal conductivity. Hence to improve the heat transfer new methodologies are developed. One such method is to append nano-sized metallic or metallic oxides in the carrier fluids. Considerable research has been done using nanofluids enclosed in different geometries. Different useful references on nanofluids are available in the monographs written by Das et al. [9], Nield and Bejan [10], Michaelides [11] and Shenoy et al. [12], and in reviews by Buongiorno et al. [13], Kakaç and Pramuanjaroenkij [14], Wong and Leon [15], Manca et al. [16], and Myers et al. [17], etc. Recently Ahmad et al. [18] studied nanofluid flow past a vertical Riga-plate subjected to convective heating. Riga-plate was composed of span wise aligned array of electrodes and permanent magnets fixed on a plane surface. They came to the conclusion that heat flux from the plate was not influenced with the variations of Brownian diffusion coefficient and utmost heat transfer rate was attained in the absence of thermophoretic effects.

Tiwari and Das [19] presented the convective flow parameters for Cu-water nanofluid within a double lid-driven square chamber. There are many different approaches that can be used for description of the nanofluid transport processes including the homogeneous (single-phase) and heterogeneous (two-phase) models. The liquid phase and the particles are treated to have heat equilibrium and negligible slip velocity in homogeneous model [20]. Using single-phase model Turkyilmazoglu [21] mathematically proved that the nanofluids cool the system as the nanoparticles volume fraction was increased for the jet flow. Turkyilmazoglu [22] also discussed slip flow in a concentric annuli adopting both single- and two-phase nanofluid models. Very recently Turkyilmazoglu [23] probed the stability analysis using single-phase model for the nanofluid. It was found that the critical Reynolds number in a traditional boundary layer flow was pushed to higher values with the dispersed nanoparticles in a working fluid. Similar results were obtained by Umavathi and her group using two-phase model to define the nanofluid behavior [24–28].

Nanofluids enclosed in a lid-driven square basin were researched by Talebi et al. [29]. The reaction of nanoparticles was reduced for large values of Reynolds number. Using Buongiorno's model Benzema et al. [30] inspected the magnetic field impact on a nanofluid in a vented trapezoidal cavity. It was revealed that the average Nusselt number increases with the nanoparticles addition, depends on the Hartmann number also. Lahlou et al. [31] pondered numerically the flow of a temperature-dependent

viscoplastic fluid containing hybrid Ag and MgO nanoparticles through a ventilated heated cavity employing extended Buongiorno's model. They revealed that the nanoparticles distribution was the same for both constituents to the dominance of inertia and buoyancy forces over slip mechanisms. Umavathi et al. [32–36] considered homogenous model to understand the energy transfer for constant and variable viscosity and thermal conductivity.

Wen and Ding [37] proved experimentally that the slip velocity was negligible between the carrier fluid and nanoparticles. Buongiorno [38] claimed that Brownian diffusion and thermophoresis are very important slip mechanisms for heterogeneous model. The Buongiorno's two-phase model was discussed by many researchers in the literature. Ouyahia et al. [39] presented the numerical solutions for the free convection of a non-Newtonian carbopol-TiO₂ nanofluid confined in a square cavity. They claimed that the nanofluid viscosity increases with the solid volume fraction and hence reduces the fluid motion and upsurges the unyielded plug size. However the thermal conductivity of the nanofluid boosts the rate of heat transfer. Umavathi [40] explained for the effects of thermal modulation using heterogeneous model for nanofluids. Alinia et al. [41] also used the two-phase model to understand the convection inside the inclined double lid-driven square chamber. They proved that SiO₂ nanoparticles cause the highest energy transfer. Cross diffusion and variable properties were introduced on the permeable nanofluid using Buongiorno's model.

Khanafer et al. [42] researched the nanofluid tendency in quadrangles. Differentially heated side walls were taken for study. Energy transfer in a rectangular vessel stuffed with nanofluid was researched by Jou and Tzeng [43] for the outcome of heat transport rate and momentum due to the presence of nanoparticles. Kherroubi et al. [44] considered the two- and three-dimensional comparative study of heat transfer and pressure drop characteristics of nanofluids flow through a ventilated cubic cavity. They derived the result that when the Reynolds number increases, the heat exchange rate was an increasing function and the pressure drop was a decreasing function. The numerical investigation of steady and laminar mixed convection flow within an irregular ventilated enclosure, crossed by Cu-water nanofluid was carried out by Benzema et al. [45]. They claimed that the heat transfer was enhanced by the increasing the nanoparticles volume fraction, Richardson and Reynolds numbers and it was suppressed by reducing the diameter of the nanoparticles. The origin of convection of Newtonian or non-Newtonian fluid in a nanoliquid saturated porous medium was discussed by Umavathi et al. [46-48].

Selecting finite element method to compute the solutions of Al₂O₃-water nanofluid confined in a porous triangular geometry was tested by Chowdhury et al. [49] for double diffusion effect. Heterogeneous model was chosen by Aly and Raizah [50] to measure the double diffusion effects by

choosing ISPH (incompressible smoothed particle hydrodynamics) method. Recently Umavathi et al. [51] inspected double-diffusion convection including cross diffusions for the porous matrix saturated by nanofluid. Umavathi and Sheremet [52] also discussed the stability for micropolar nanofluid using heterogeneous model for double diffusions. Kuznetsov and Nield [53] and Nield and Kuznetsov [54] measured double diffusions over boundary layer flows analytically.

There are considerable researches on the nanoliquids energy transport that highlight totally different results. Investigators [55–57] claim that energy is improved by suspending nano-sized solid particles because the presence of particles increases the thermal conductivity.

However, some researchers also declare that the spreading of nanoparticles in the carrier fluid results in the decline of energy [58, 59]. The theoretical findings for free convection in chambers are controversial with the experiments. As a result, assumptions used in the theoretical approaches can lead to questionable results. The nanoliquids energy augmentation also may be due to the formulae employed for their physical characteristics. A comprehensive nanoliquid modelling investigation should consider the structure, shape, size, fabrication process, particle aggregation and deterioration of nanofluids. Recently Diglio et al. [60] studied both numerically and experimentally borehole heat exchanger with nanofluids as heat carrier.

Since the experimental and numerical results for free convection in enclosures are controversial, the authors have been motivated to explore more light on this issue. Surveying the previous publications and to the authors best knowledge, that there has been no publications of research dealing with the double diffusion using the monophasic model, by taking into account both the Soret and Dufour effects and viscous dissipation which cause the rise of the bulk temperature. Therefore, the central motto of the present investigation is to initiate the numerical study for the double diffusive convective nanofluid flow along with dissipations caused by viscosity in a rectangular duct.

2. Mathematical model

A graphic of the geometry under study is delineated in Fig. 1. The left plate is kept at temperature T_1 and right plate is heated at T_2 such that $T_2 > T_1$. The concentration at the right plate is higher than the left wall ($C_2 > C_1$). The other walls are adiabatic and impermeable. The water-based nanoliquid including various nanoparticles with Soret and Dufour effects is within the duct. The nanofluid motion is considered to be steady, laminar and incompressible. Homogeneous model for the nanofluid is considered along with constant physical properties. The Boussinesq approximation is also incorporated. Buoyancy force drives free convection. Inertial force and terms of convection (in the energy and

diffusion equation) are neglected and uniform pressure is applied in the rectangular enclosure [32, 42, 43] so that

$$U = V = 0, \quad \frac{\partial U}{\partial X} = \frac{\partial U}{\partial Y} = \frac{\partial V}{\partial X} = \frac{\partial V}{\partial Y} = 0, \quad \frac{\partial P}{\partial X} = \frac{\partial P}{\partial Y} = \frac{\partial P}{\partial Z} = 0 \quad (1)$$

By conservation of mass, we derive $\partial W/\partial Z = 0$ which suggest that W does not depend on Z , i.e. $W = W(X, Y)$.

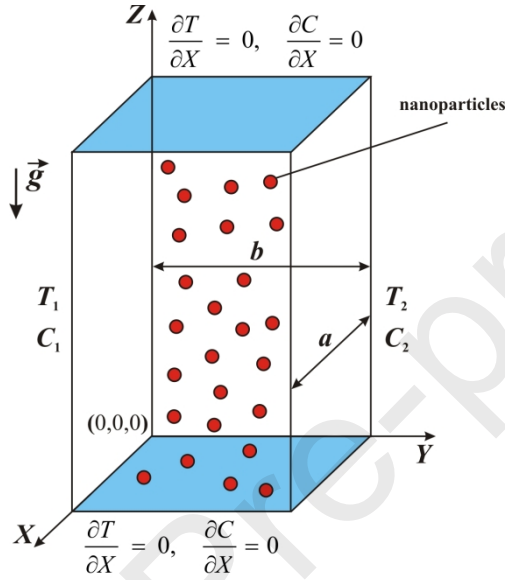


Figure 1. Physical configuration.

Enforcing the above hypothesis, the momentum, energy and concentration balance equations are

$$\mu_{nf} \left(\frac{\partial^2 W}{\partial X^2} + \frac{\partial^2 W}{\partial Y^2} \right) + g(\rho\beta)_{nf} [(T - T_0) - \gamma(C - C_0)] = 0 \quad (2)$$

$$\frac{\partial^2 T}{\partial X^2} + \frac{\partial^2 T}{\partial Y^2} + \frac{\mu_{nf}}{K_{nf}} \left(\left(\frac{\partial W}{\partial X} \right)^2 + \left(\frac{\partial W}{\partial Y} \right)^2 \right) + \frac{D K_{Tf}}{C_s C_p \alpha_{nf}} \left(\frac{\partial^2 C}{\partial X^2} + \frac{\partial^2 C}{\partial Y^2} \right) = 0 \quad (3)$$

$$\frac{\partial^2 C}{\partial X^2} + \frac{\partial^2 C}{\partial Y^2} + \frac{K_{Tf}}{T_m} \left(\frac{\partial^2 T}{\partial X^2} + \frac{\partial^2 T}{\partial Y^2} \right) = 0 \quad (4)$$

Equations (2)–(4) are worked out using additional border conditions:

$$\begin{aligned} W=0, \quad T=T_1, \quad C=C_1 \quad & \text{at } Y=0 \quad \text{for } 0 \leq X \leq a \\ W=0, \quad T=T_2, \quad C=C_2 \quad & \text{at } Y=b \quad \text{for } 0 \leq X \leq a \\ W=0, \quad \frac{\partial T}{\partial X} = 0, \quad \frac{\partial C}{\partial X} = 0 \quad & \text{at } X=0 \quad \text{for } 0 \leq Y \leq b \\ W=0, \quad \frac{\partial T}{\partial X} = 0, \quad \frac{\partial C}{\partial X} = 0 \quad & \text{at } X=a \quad \text{for } 0 \leq Y \leq b \end{aligned} \quad (5)$$

The nanofluid relations enabled are

$$\rho_{nf} = (1-\Phi)\rho_f + \Phi\rho_s \quad (6)$$

$$(\rho C_p)_{nf} = (1-\Phi)(\rho C_p)_f + \Phi(\rho C_p)_s \quad (7)$$

$$(\rho\beta)_{nf} = (1-\Phi)(\rho\beta)_f + \Phi(\rho\beta)_s \quad (8)$$

$$\alpha_{nf} = \frac{K_{nf}}{(\rho C_p)_{nf}} \quad (9)$$

$$\mu_{nf} = \frac{\mu_f}{(1-\Phi)^{2.5}} \quad (10)$$

The relation in Eq. (10) is the Brinkman model for the effective viscosity [61].

For a spherical nanoparticle, the Maxwell relation [62] is opted

$$K_{nf} = K_f \left(\frac{K_s + 2K_f - 2\Phi(K_f - K_s)}{K_s + 2K_f + \Phi(K_f - K_s)} \right) \quad (11)$$

The above equations are non-dimensionalized by selecting the following relations

$$\begin{aligned} x = \frac{X}{b}, \quad y = \frac{Y}{b}, \quad w = \frac{W\rho_f b}{\mu_f}, \quad \theta = \frac{T - T_0}{T_2 - T_1}, \quad c = \frac{C - C_0}{C_2 - C_1}, \quad T_0 = \frac{T_1 + T_2}{2}, \\ C_0 = \frac{C_1 + C_2}{2}, \quad GrT = \frac{g\beta_T(T_2 - T_1)b^3\rho_f^2}{\mu_f^2}, \quad GrC = \frac{g\beta_C(C_2 - C_1)b^3\rho_f^2}{\mu_f^2}, \\ Br = \frac{\mu_f^3}{K_f\rho_f^2 b^2(T_2 - T_1)}, \quad Pr = \left(\frac{\nu}{\alpha} \right)_f, \quad D_f = \left(\frac{D}{\nu} \right)_f \frac{K_{Tf}(C_2 - C_1)}{C_s C_p(T_2 - T_1)}, \\ Sr = \left(\frac{D}{\nu} \right)_f \frac{K_{Tf}(T_2 - T_1)}{T_m(C_2 - C_1)}, \quad Sc = \left(\frac{\nu}{D} \right)_f \end{aligned} \quad (12)$$

The reduced dimensionless governing equations are

$$\frac{\partial^2 w}{\partial x^2} + \frac{\partial^2 w}{\partial y^2} + GrT(1-\Phi)^{2.5} \left(1 - \Phi + \Phi \frac{(\rho\beta)_s}{(\rho\beta)_f} \right) \theta - GrC(1-\Phi)^{2.5} \left(1 - \Phi + \Phi \frac{(\rho\beta)_s}{(\rho\beta)_f} \right) c = 0 \quad (13)$$

$$\frac{\partial^2 \theta}{\partial x^2} + \frac{\partial^2 \theta}{\partial y^2} + \frac{Br}{(1-\Phi)^{2.5}} \left(\frac{K_s + 2K_f + \Phi(K_f - K_s)}{K_s + 2K_f - 2\Phi(K_f - K_s)} \right) \left(\left(\frac{\partial w}{\partial x} \right)^2 + \left(\frac{\partial w}{\partial y} \right)^2 \right) + \quad (14)$$

$$D_f Pr \frac{\alpha_f}{\alpha_{nf}} \left(\frac{\partial^2 c}{\partial x^2} + \frac{\partial^2 c}{\partial y^2} \right) = 0$$

$$\frac{\partial^2 c}{\partial x^2} + \frac{\partial^2 c}{\partial y^2} + Sr \cdot Sc \left(\frac{\partial^2 \theta}{\partial x^2} + \frac{\partial^2 \theta}{\partial y^2} \right) = 0 \quad (15)$$

The correlative conditions on the boundaries become

$$\begin{aligned}
 w=0, \quad \theta=-0.5, \quad c=-0.5 \quad \text{at} \quad y=0 \quad \text{for} \quad 0 \leq x \leq A \\
 w=0, \quad \theta=0.5, \quad c=0.5 \quad \text{at} \quad y=1 \quad \text{for} \quad 0 \leq x \leq A \\
 w=0, \quad \frac{\partial \theta}{\partial x}=0, \quad \frac{\partial c}{\partial x}=0 \quad \text{at} \quad x=0 \quad \text{and} \quad x=A \quad \text{for} \quad 0 \leq y \leq 1
 \end{aligned} \tag{16}$$

The parameters including volumetric circulation strength, skin friction, Nusselt number and Sherwood number are evaluated with copper nanoparticle and water as a carrier fluid and exhibited in Tables 2 to 5.

3. Computational procedure

Equations (13) to (16) are solved through the application of finite difference technique. Central differences of second-order accuracy are used to constitute the finite difference equations to the first- and second-order derivatives. As a result, the final difference equations are

$$\frac{w_{i+1,j} - 2w_{i,j} + w_{i-1,j}}{(\Delta x)^2} + \frac{w_{i,j+1} - 2w_{i,j} + w_{i,j-1}}{(\Delta y)^2} + GrT(1-\Phi)^{2.5} \left(1 - \Phi + \Phi \frac{(\rho\beta)_s}{(\rho\beta)_f} \right) \theta_{i,j} - \tag{17}$$

$$GrC(1-\Phi)^{2.5} \left(1 - \Phi + \Phi \frac{(\rho\beta)_s}{(\rho\beta)_f} \right) c_{i,j} = 0$$

$$\begin{aligned}
 & \frac{\theta_{i+1,j} - 2\theta_{i,j} + \theta_{i-1,j}}{(\Delta x)^2} + \frac{\theta_{i,j+1} - 2\theta_{i,j} + \theta_{i,j-1}}{(\Delta y)^2} + \\
 & \frac{Br}{(1-\Phi)^{2.5}} \left(\frac{K_s + 2K_f + \Phi(K_f - K_s)}{K_s + 2K_f - 2\Phi(K_f - K_s)} \right) \left(\left(\frac{w_{i+1,j} - w_{i-1,j}}{2\Delta x} \right)^2 + \left(\frac{w_{i,j+1} - w_{i,j-1}}{2\Delta y} \right)^2 \right) + \tag{18}
 \end{aligned}$$

$$D_f Pr \frac{\alpha_f}{\alpha_{nf}} \left(\frac{c_{i+1,j} - 2c_{i,j} + c_{i-1,j}}{(\Delta x)^2} + \frac{c_{i,j+1} - 2c_{i,j} + c_{i,j-1}}{(\Delta y)^2} \right) = 0$$

$$\begin{aligned}
 & \frac{c_{i+1,j} - 2c_{i,j} + c_{i-1,j}}{(\Delta x)^2} + \frac{c_{i,j+1} - 2c_{i,j} + c_{i,j-1}}{(\Delta y)^2} + \\
 & Sr \cdot Sc \left(\frac{\theta_{i+1,j} - 2\theta_{i,j} + \theta_{i-1,j}}{(\Delta x)^2} + \frac{\theta_{i,j+1} - 2\theta_{i,j} + \theta_{i,j-1}}{(\Delta y)^2} \right) = 0 \tag{19}
 \end{aligned}$$

Applying the ghost cells technique, the boundary conditions (16) on the plates become:

The relevant conditions on the plates become

$$\begin{aligned}
w_{i,0} &= -w_{i,1}, \quad \theta_{i,0} = -1 - \theta_{i,1}, \quad c_{i,0} = -1 - c_{i,1} \\
w_{i,Ny+1} &= -w_{i,Ny}, \quad \theta_{i,Ny+1} = 1 - \theta_{i,Ny}, \quad c_{i,Ny+1} = 1 - c_{i,Ny} \\
w_{0,j} &= -w_{1,j}, \quad \theta_{0,j} = \theta_{1,j}, \quad c_{0,j} = c_{1,j} \\
w_{Nx+1,j} &= -w_{Nx,j}, \quad \theta_{Nx+1,j} = \theta_{Nx,j}, \quad c_{Nx+1,j} = c_{Nx,j}
\end{aligned} \tag{20}$$

Here i and j represent the divisions from 1 to Nx (nodes for x axis) and 1 to Ny (nodes for y axis), respectively. The discretized algebraic equations are iteratively solved. For the convergence Southwell-Over-Relaxation technique is enforced. The velocity, energy and concentration solutions are stopped after considering that at any grid point the two consecutive iterations are less than the tolerance value which is chosen to be 10^{-14} . The numerical method is validated by grid-independence study. The heat transport rate and friction at the plates of the conduit are decided using 10×10 , 50×50 , 100×100 , 150×150 and 200×200 grids and are delineated in Table 1. The solutions for 50×50 , 100×100 , 150×150 and 200×200 grids are quite similar. In the absence of concentration $GrC = 0$, $Df = 0$, $Sr = 0$, the results agree with Umavathi et al. [32] (see Table 6).

The temperature contours for the ramification on Φ , Df , Br , and Sr are similar to GrC and hence not reproduced in figures. The implement of GrT , GrC , Φ , Df , Br and Sr on the concentration curves produces the similar nature as that on the temperature contours and hence not detailed in the form of diagrams.

4. Results and discussion

We discuss the outcomes of different model parameters. We also explore the friction and heat transport rate at the plates using five different nanoparticles. The parameter ranges we consider are $1 \leq GrT \leq 20$, $1 \leq GrC \leq 15$, $0 \leq \Phi \leq 0.05$, $0 \leq Df \leq 1$, $0 \leq Br \leq 2$, $0 \leq Sr \leq 5$, $0 \leq Sc \leq 5$, $0.5 \leq A \leq 2$. The effects of copper, SiO_2 , silver, TiO_2 , diamond as nanoparticles and water as carrier fluid were also evaluated. The results are reproduced in plots and tables. Using MATLAB software the plots in three- and two-dimension forms are represented. The pictures are also demonstrated in one-dimension form varying x from 0 to 1 and fixing y at 0.5 (midpoint of the duct) to detail a better insight for the estimation on the flow field. For all the graphs and tables the values are taken as $GrT = 10$, $GrC = 5$, $\Phi = 0.05$, $Df = 1.0$, $Br = 1.0$, $Pr = 7.0$, $Sr = 2.0$, $Sc = 5.0$, $A = 1.0$ except the varying one.

The velocity, temperature and concentration fields for particular nanofluids are notified in Figs. 2a and 2b. It is looked from Fig. 2a (3D graphs) that the velocities in the upward direction ($y > 0.5$) and in the downward direction ($y < 0.5$) are steady with any of the nanoparticles. The temperature and concentration fields decrease linearly from the top plate ($y = 1$) to the bottom one

($y = 0$). It is monitored from Fig. 2a that the number of contours on the velocity, heat and concentration are unvarying for copper, diamond and silver nanoparticles. Since Fig. 2a could not fetch any information for using different nanoparticles, one-dimensional graphs are shown in Fig. 2b. It is goggled from Fig. 2b that the velocity attains the extent using silver nanoparticles and littlest using diamond nanoparticles, the energy profiles are apex for SiO_2 and fewest for diamond nanoparticles, whereas concentration profiles attains the peak for Diamond and tiniest for SiO_2 nanoparticles. However, the direction of profiles for temperature filed is opposite to that of concentration filed.

Variation of thermal Grashof number GrT are plotted in Figs. 3a and 3b using copper as nanoadditives and water as host liquid. The influence of GrT escalated the velocity in the downward and upward directions. The curves for the duct zone ($y < 0.5$) become sparse, while in the area of the duct ($y > 0.5$) it becomes dense as GrT increases. The GrT when gazed on the temperature field resulted that there is remarkable deviation as GrT increases. For the value of $GrT = 20$, the contour become convex and the temperature become nonlinear (Fig. 3a). The concentration contours also are immutable for the varying GrT and hence not traced on graphs. Figure 3b when glanced tells that the velocity and energy profiles gain the momentum whereas the concentration fields loose the momentum for variation of GrT .

The concentration Grashof number influence on the circulation is diagramed in Figs. 4a and 4b. The GrC shows symmetric nature in the upward and downward directions for lesser values, when hiked ($GrC = 10$) the convection cell is reduced from two-cell mode to one-cell mode, and when GrC is still boosted the convection cells again become two-cell but the consequence of the velocity field is reduced in the downward and upward directions. The temperature field does not procure distinguishable effectiveness. Similar glimpses are noticed on the concentration field also for the upper limits of GrC and hence not delineated. The sketch of GrC (Fig. 4b) in one-dimensional form is remarked. The velocity and concentration profiles are truncated by expanding GrC whereas the temperature was upsurges.

Figure 5a and 5b model the response of volume fraction Φ . The magnitudes of velocity field in the downward and upward are almost symmetric by raising the solid volume fraction. The velocity and temperature contours are consistent. When viewed keeping y fixed and varying x (Fig. 5b) enumerate that the velocity and temperature figures are subsidized but the concentration sketches are amplified. The nature of the solid volume fraction physically can be elucidated as introducing nanoadditivs to pure viscous liquid results in suspension of nanoparticles which becomes the similar physical model as that of non-Newtonian fluid. Hence including nanoparticles further to a carrier liquid results to the highly viscous fluid cause the flow to crumble.

The effect of Dufour number on the momentum and thermal fields are released in Figs. 6a and 6b. Figure 6a outlines that the momentum and thermal contours are deviated with Dufour parameter. However, when viewed at single point ($y = 0.5$), it is delineated that the momentum and heat profiles are lessening whereas the concentration profiles are enlarged.

Figure 7a and 7b narrate the influence of Brinkman number. The characteristic of Brinkman number estimates the relation between the heat generated by dissipation and heat exchanged at the walls. Incrementing the Brinkman number leads for the upsurge of momentum in the upward direction ($y > 0$) of the duct. The velocity contours are symmetric for $Br = 0$ at the middle of the duct ($y = 0.5$) and as Br rises, the velocity curves are incremented in the top area of the duct ($y > 0.5$). The temperature profiles are motionless for the outcome of Br and the contours are almost linear. This property can be justified as there is insulation at the top and bottom plates. Figure 7b manifests that the momentum and temperature profiles are amplified and the concentration profiles are contracted for the response of Br .

The Soret parameter is applied on the velocity field (Fig. 8a). The velocity field is expanded in the top half area of the duct. The velocity profiles are also condensed in the top half area of the duct for enlargement of Soret parameter. The Soret parameter alters the temperature contours and the contours are almost linear both in the upper and lower area of the duct. Figure 8b outlines that the velocities and temperatures are escalated whereas the concentration profiles are contracted. The Schmidt parameter also reports the identical chart on the flow and hence not presented.

The circulation strength and skin friction for various physical characteristics are outlined in Tables 3 and 4. It is reported that diamond nanoparticles have the declined volumetric flow rate whereas silver upswing volumetric flow rate compared with copper, TiO_2 and SiO_2 nanoparticles. Further Table 3 also sums up that the volumetric flow rate is amplified for GrT , GrC , Br , Sr , Sc , A and it is receded with Φ , Df . The skin friction dw/dy at $y = 0$ characterizes the gain for silver nanoparticles, dropped for SiO_2 nanoparticle. The influence of GrT , GrC , Df , A is to hike the skin friction and Φ , Br , Sr , Sc is to lessen the skin friction. The skin friction dw/dy at $y = 1$ upsurges for silver nanoparticles whereas it is softened for Diamond nanoparticles. The skin friction is enlarged for GrT , GrC , Br , Sr , Sc , A and contracted for Φ , Df .

The shear stress dw/dx at $x = 0$ and $x = 1$ accomplished upper limit for silver nanoparticles and lower limit for diamond nanoparticles in magnitude. The skin friction at $x = 0$ and at $x = 1$ upswings with GrT , GrC , Br , Sr , Sc , A whereas it slackens with Φ , Df in magnitude.

The heat transfer rate $d\theta/dy$ at $y=0$ achieved apex value for silver nanoparticles and abate value for SiO_2 nanoparticles as seen in Table 4. Diamond nanoparticles gained the best value and SiO_2 nanoparticles get the weakened value for the energy transport strength at $y=1$. The energy transport strength at $y=0$ is amplified with GrT , Φ , Df , Br , A whereas it crumbled with GrC , Sr , Sc . At the right wall, the heat transfer rate is degenerated with GrT , Br , Sr , Sc , A whereas it is accelerated with GrC , Φ , Df .

The numbers obtained for Sherwood parameter dc/dy at $y=0$ and at $y=1$ are available in Table 5. Diamond nanoparticles reach the optimal values whereas SiO_2 nanoparticles earn the minimal Sherwood number at $y=0$ whereas the opposite effect is realized for the Sherwood number at $y=1$. The dimensionless parameters GrT , Df , Br , Sr , Sc , A diminish the Sherwood number at $y=0$ and GrC , Φ expand the Sherwood number. The Sherwood number at the right plate gets larger for GrT , Br , Sr , Sc , A whereas it is lowered for GrC , Φ , Df .

5. Conclusions

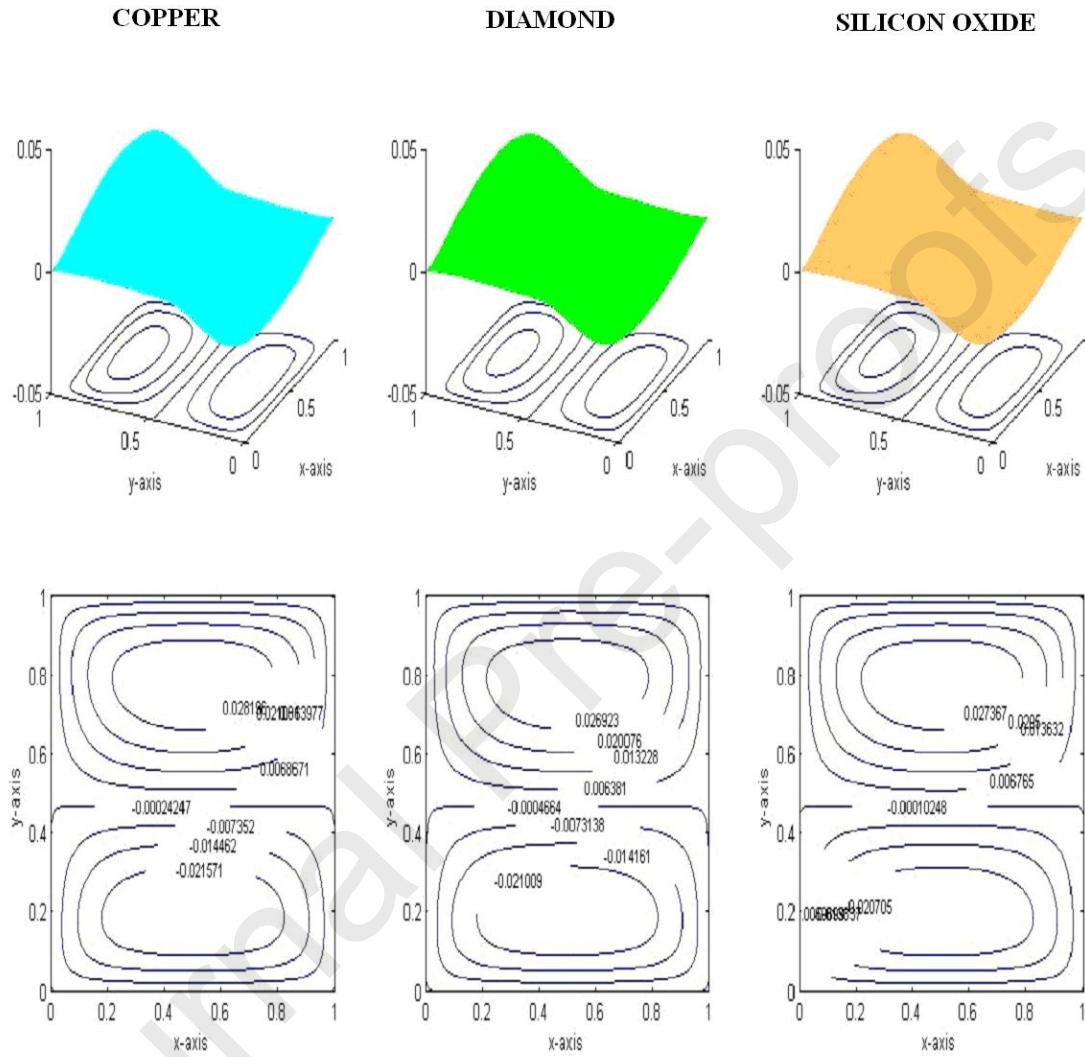
The buoyancy-driven nanoliquid convection within a rectangular conduit with viscous warming was discussed incorporating double diffusions using the single-phase nanoliquid approach. The control equations were worked out by the finite difference technique. From the computations it was concluded that

1. The velocity was maximum using silver nanoparticles and lowest using diamond nanoparticles. The temperature is high for silicon oxide nanoparticles and low for diamond nanoparticles and opposite effect was obtained for concentration.

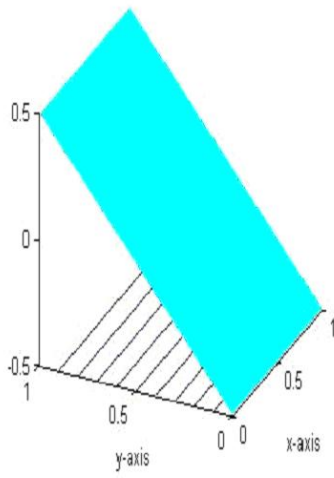
2. Thermal Grashof, Brinkman, Dufour, Soret and Schmidt parameters increase the velocity and temperature and these dimensionless parameters decrease the concentration whereas the reversal effect was obtained for the solid volume fraction. The velocities and temperatures were reduced and concentration was improved by concentration Grashof parameter. However the temperature contours are not changed significantly on nanoparticles, concentration Grashof number, solid volume fraction, Brinkman, Dufour, Soret and Schmidt parameters.

3. The energy transport strength at the left border attained the peak for silver nanoparticles and least for silicon oxide nanoparticles. At the right plate diamond nanoparticles proved the best and silicon oxide nanoparticles to be less effective. GrT , Φ , Df , Br amplify and GrC , Sr , Sc will lower the heat transport rate at $y=0$. GrT , GrC , Φ , Df amplify and GrT , Br , Sr , Sc degenerate the heat rate at

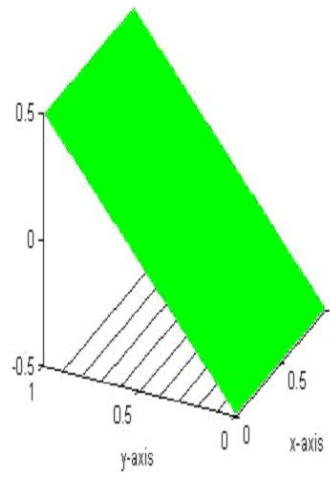
$y = 1$. The Sherwood number at $y = 0$ was crumbled with GrT , Df , Br , Sr , Sc , A and was hiked with GrC , Φ . At $y = 1$, it was enlarged with GrT , Br , Sr , Sc , A and was lowered with GrC , Φ , Df .



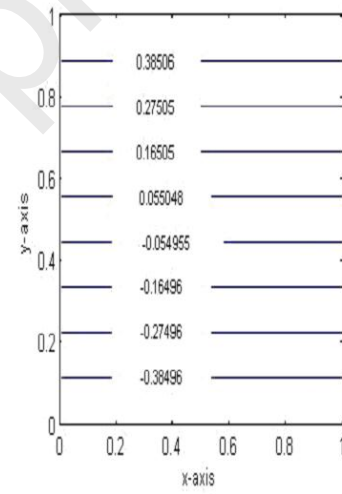
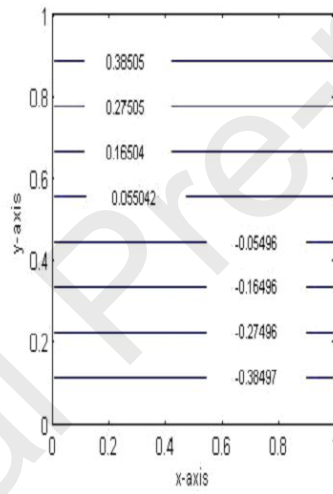
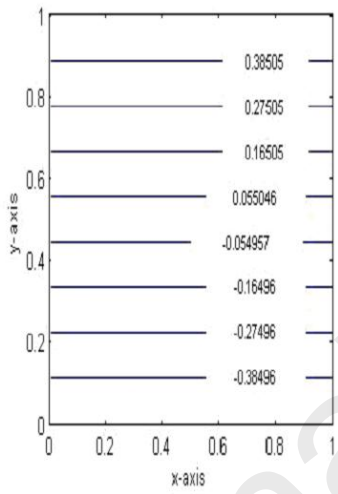
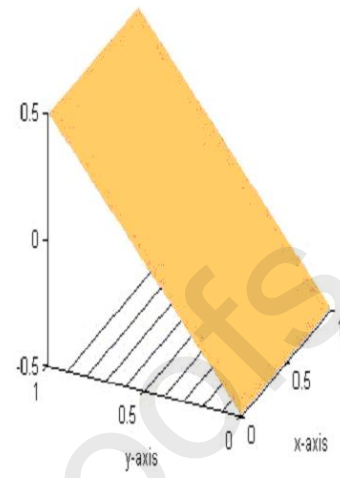
COPPER



DIAMOND



SILICON OXIDE



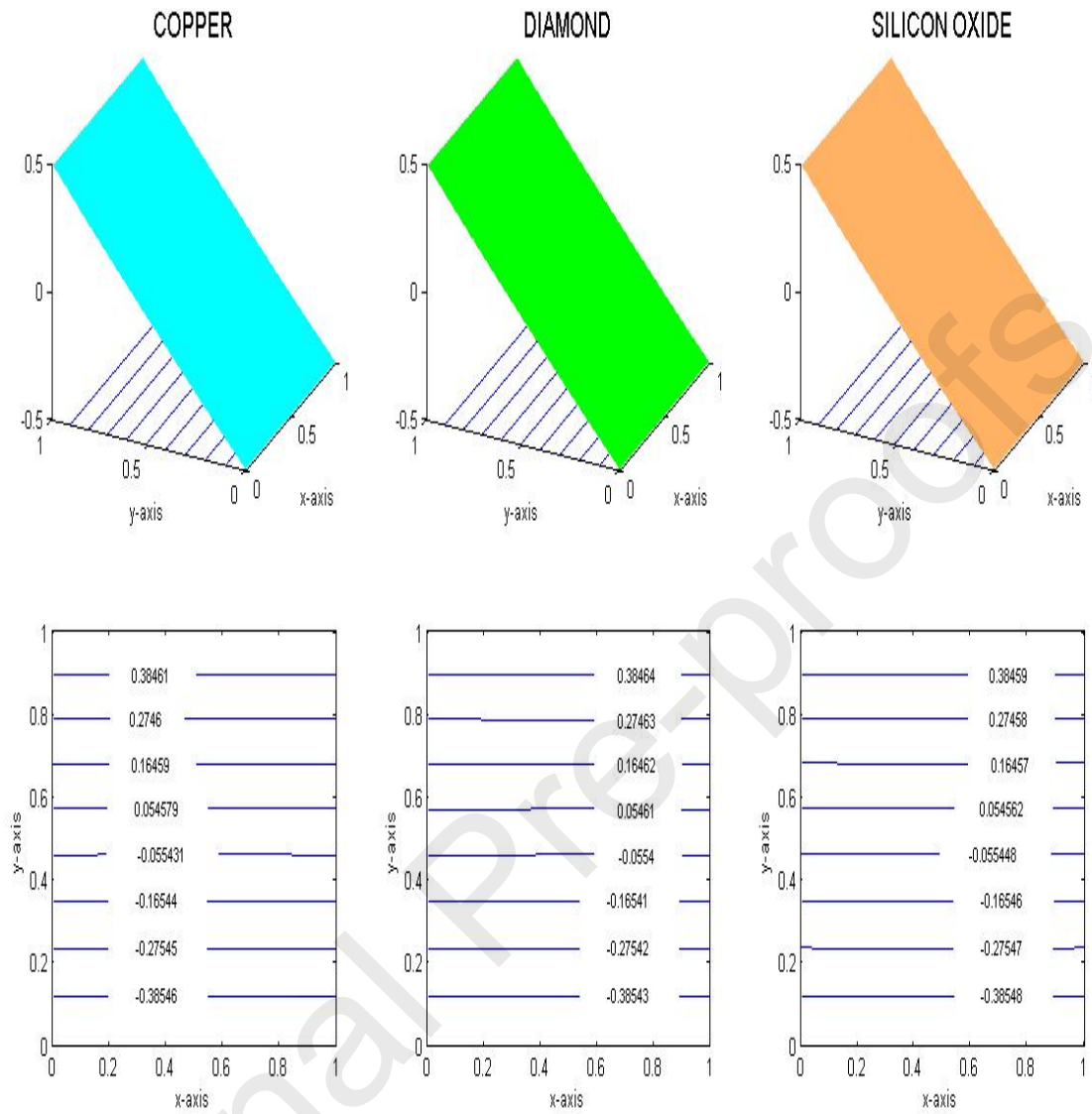
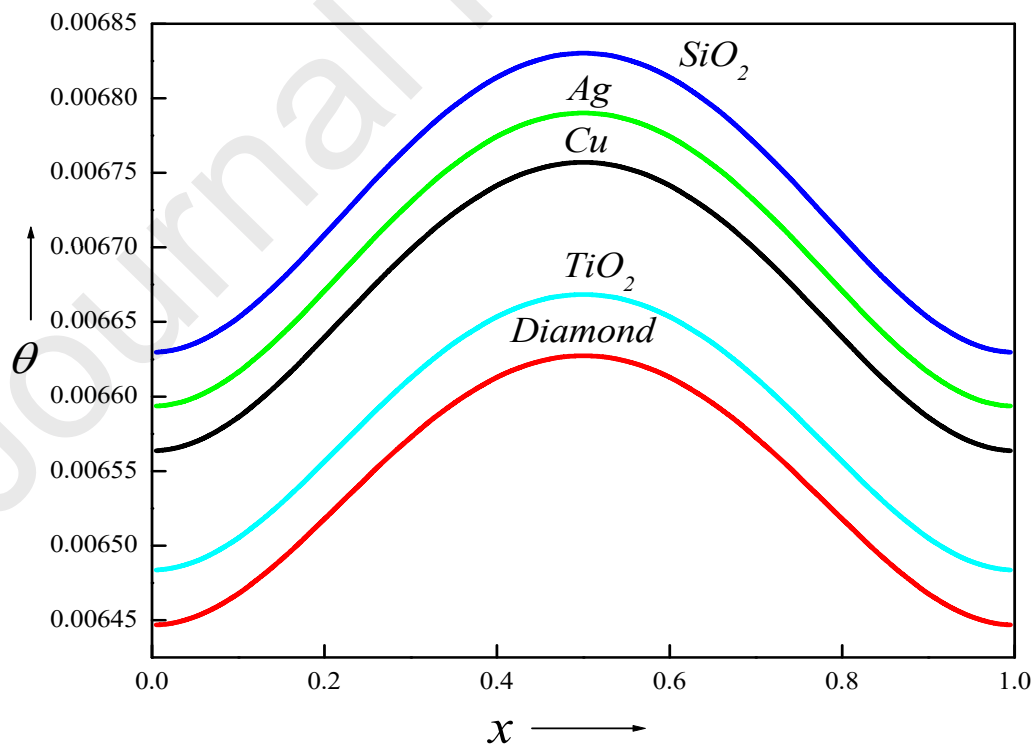
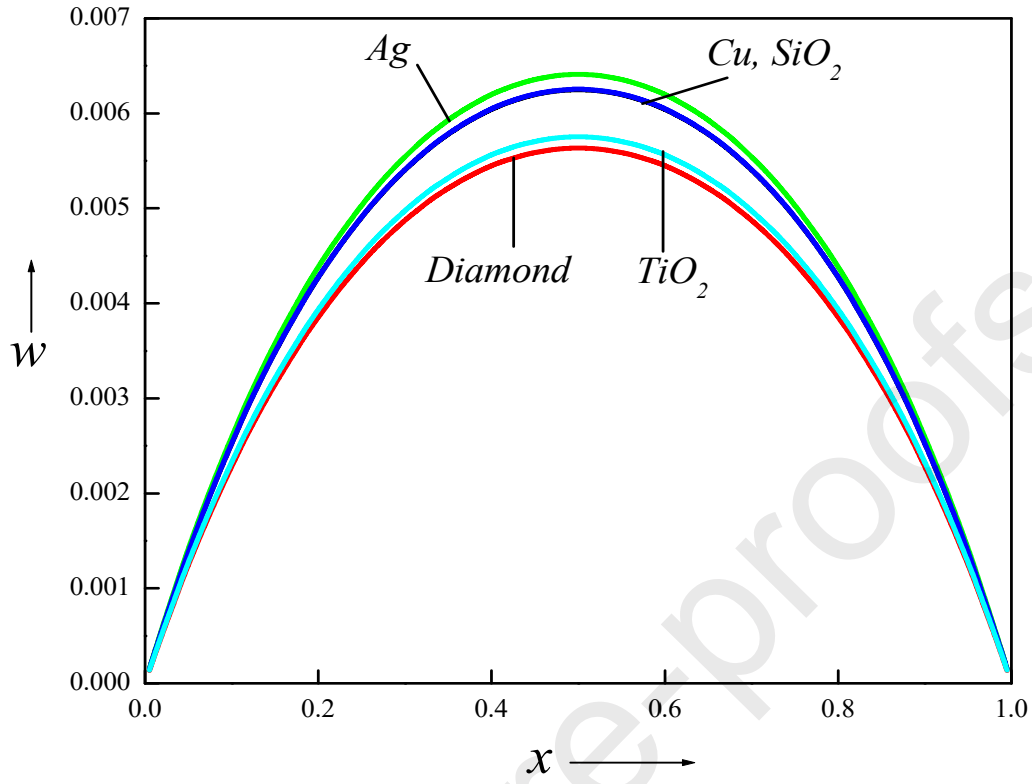


Figure 2a. Isocontours of velocity, temperature and concentration using different nanoparticles.



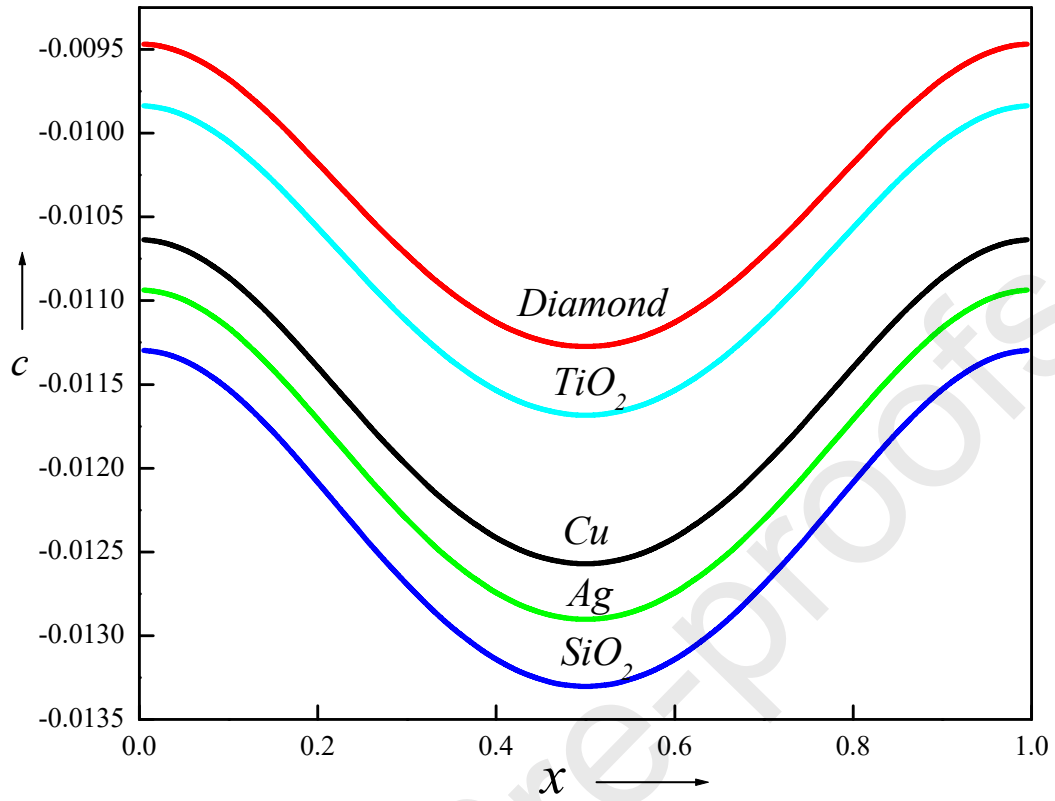
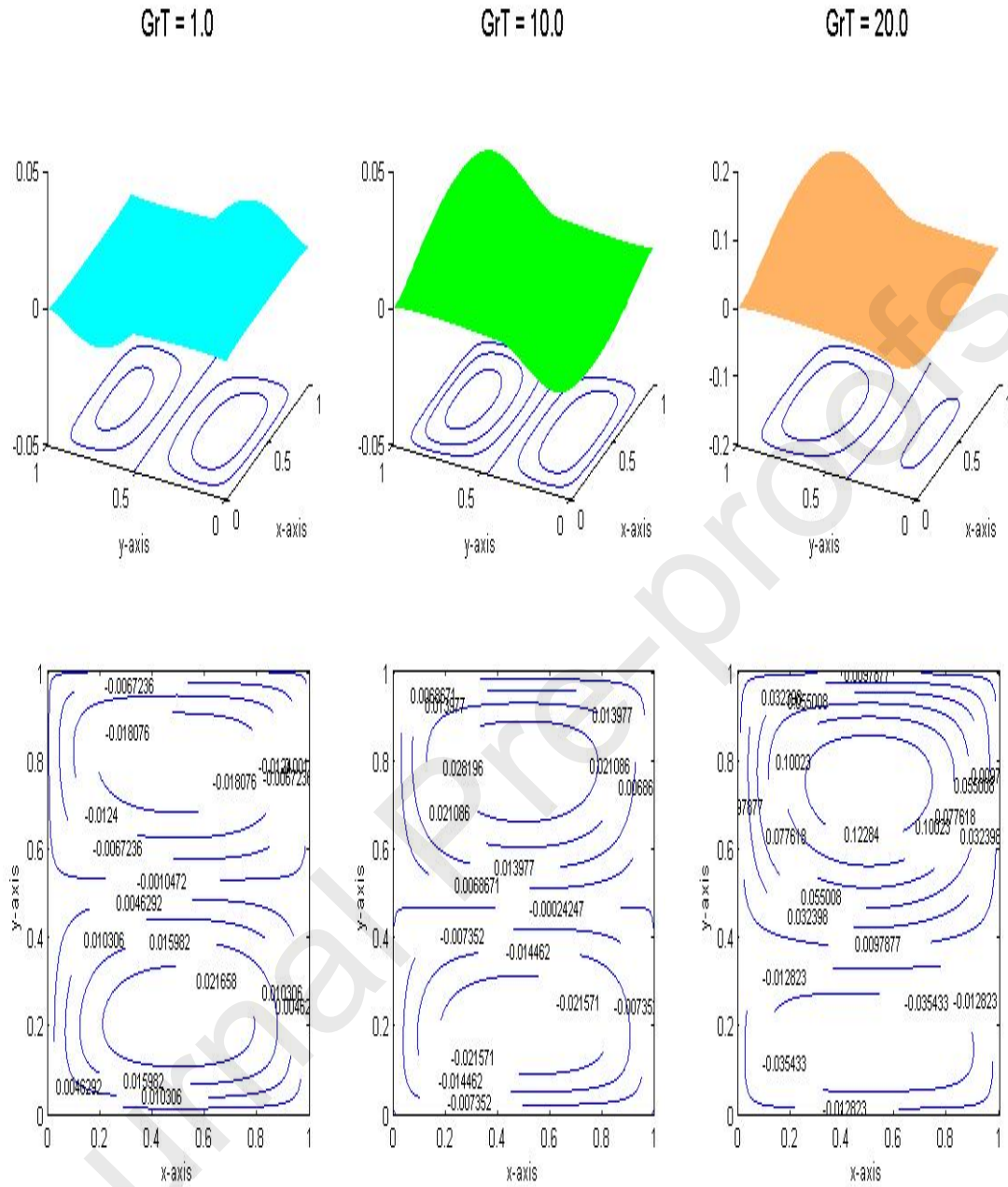


Figure 2b. Profiles of velocity, temperature and concentration using different nanoparticles.



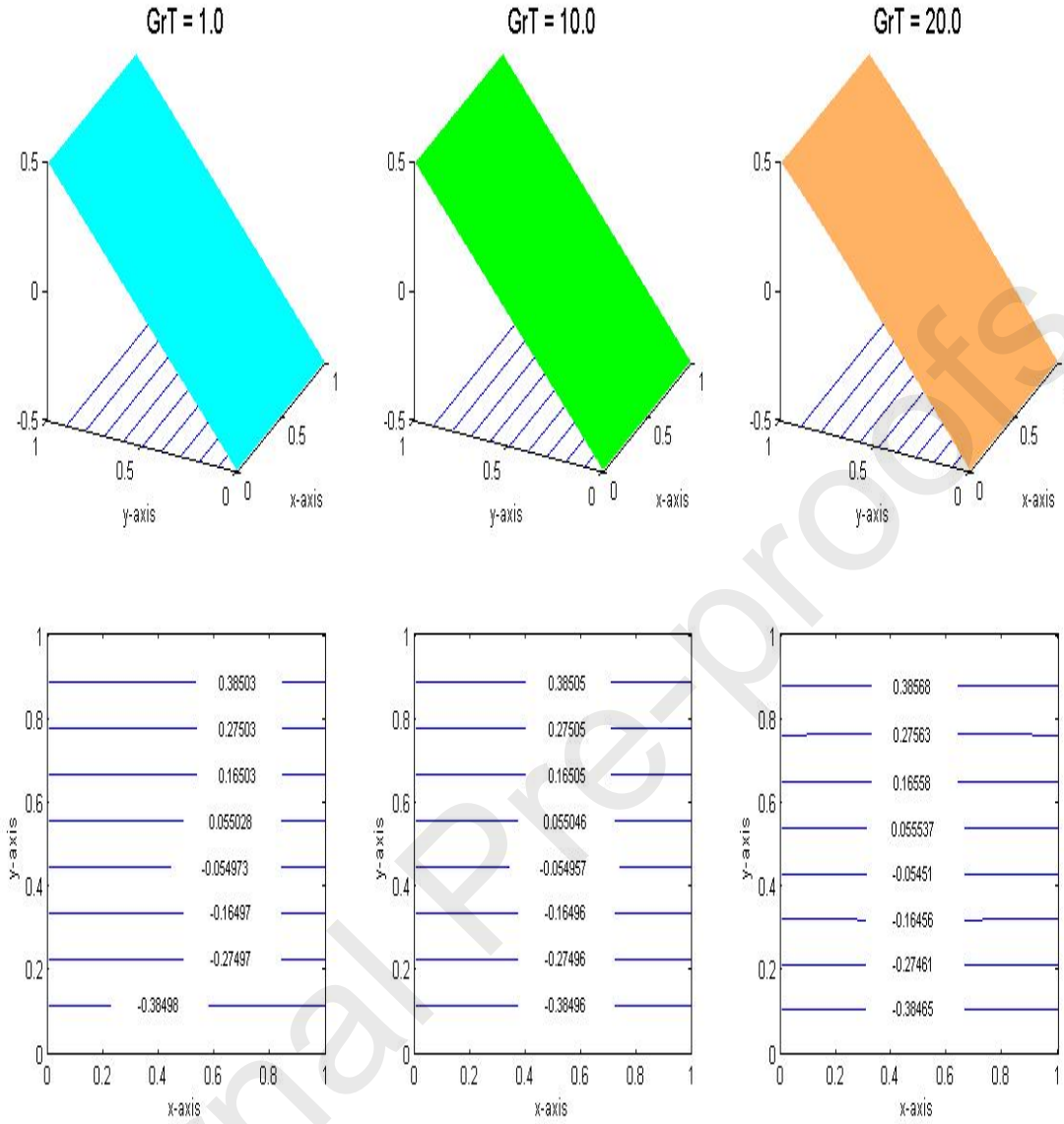
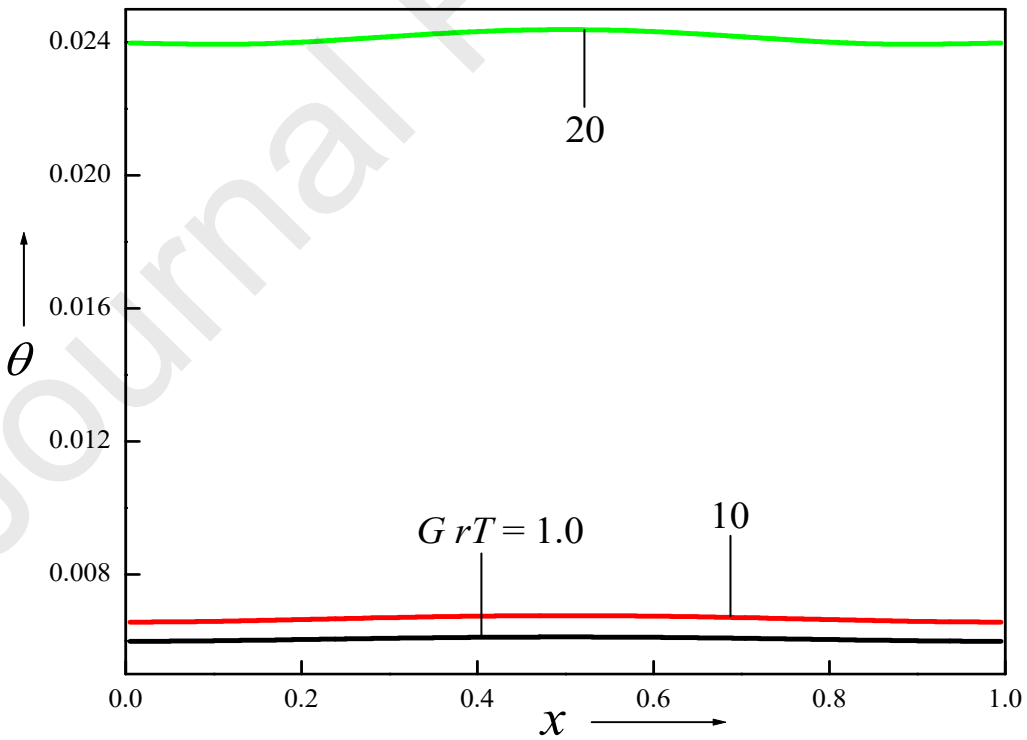
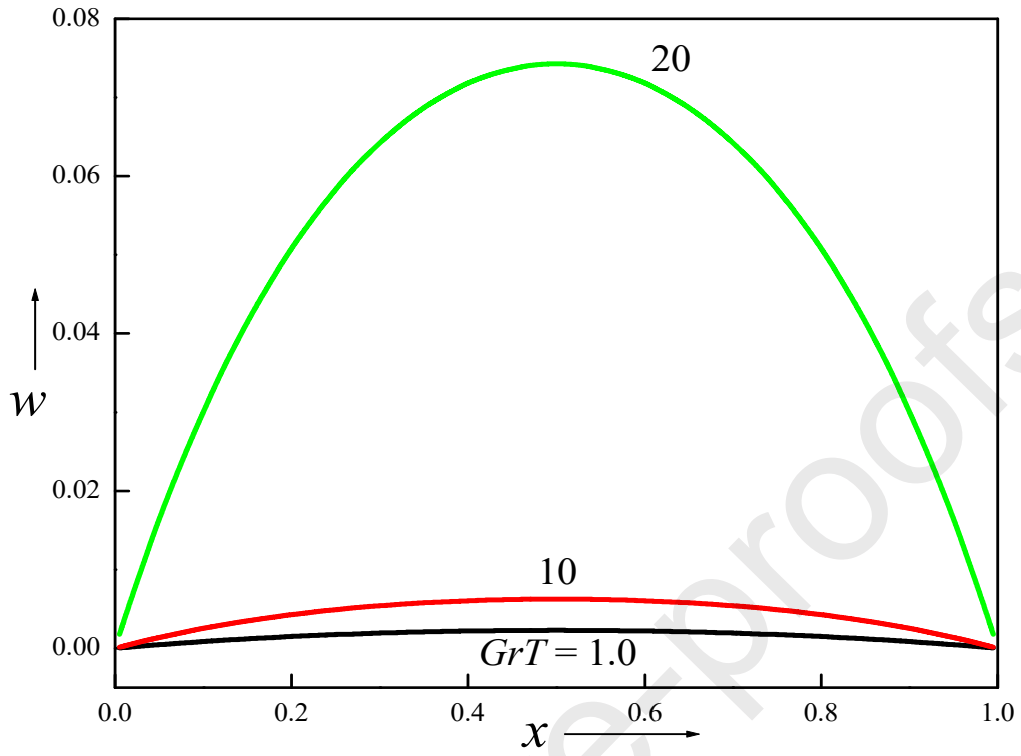


Figure 3a. Isocontours of velocity and temperature for distinct GrT .



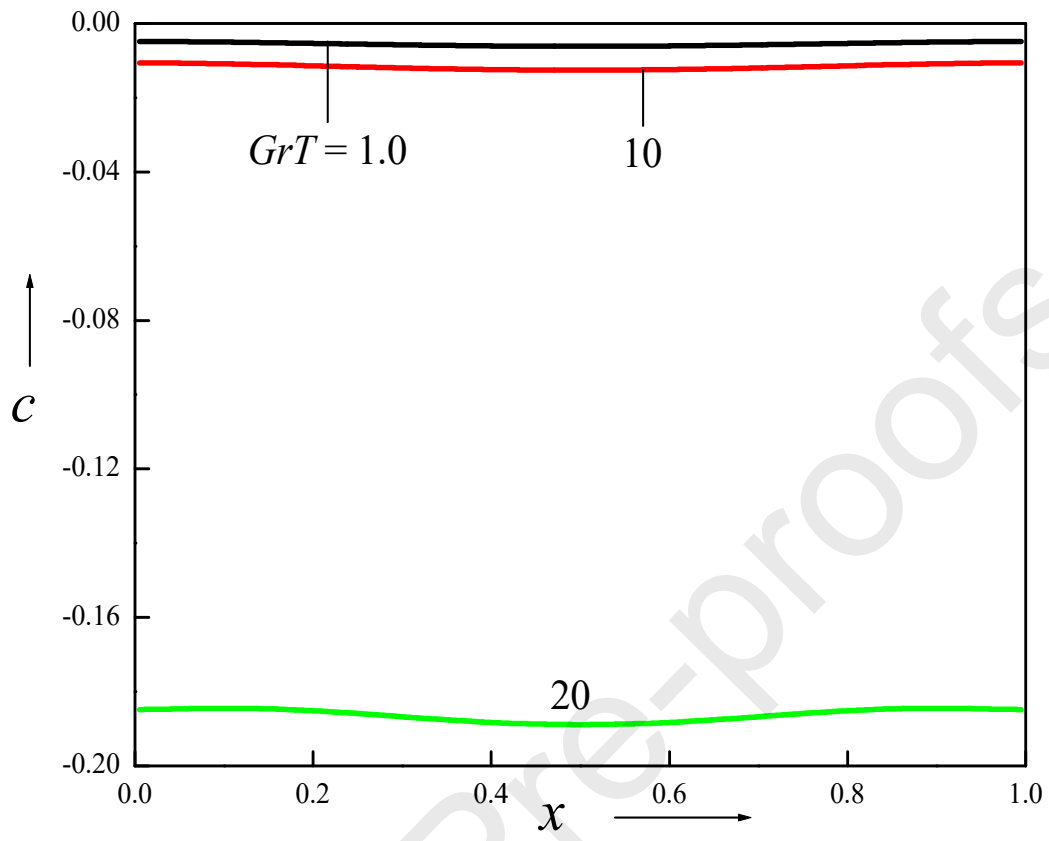
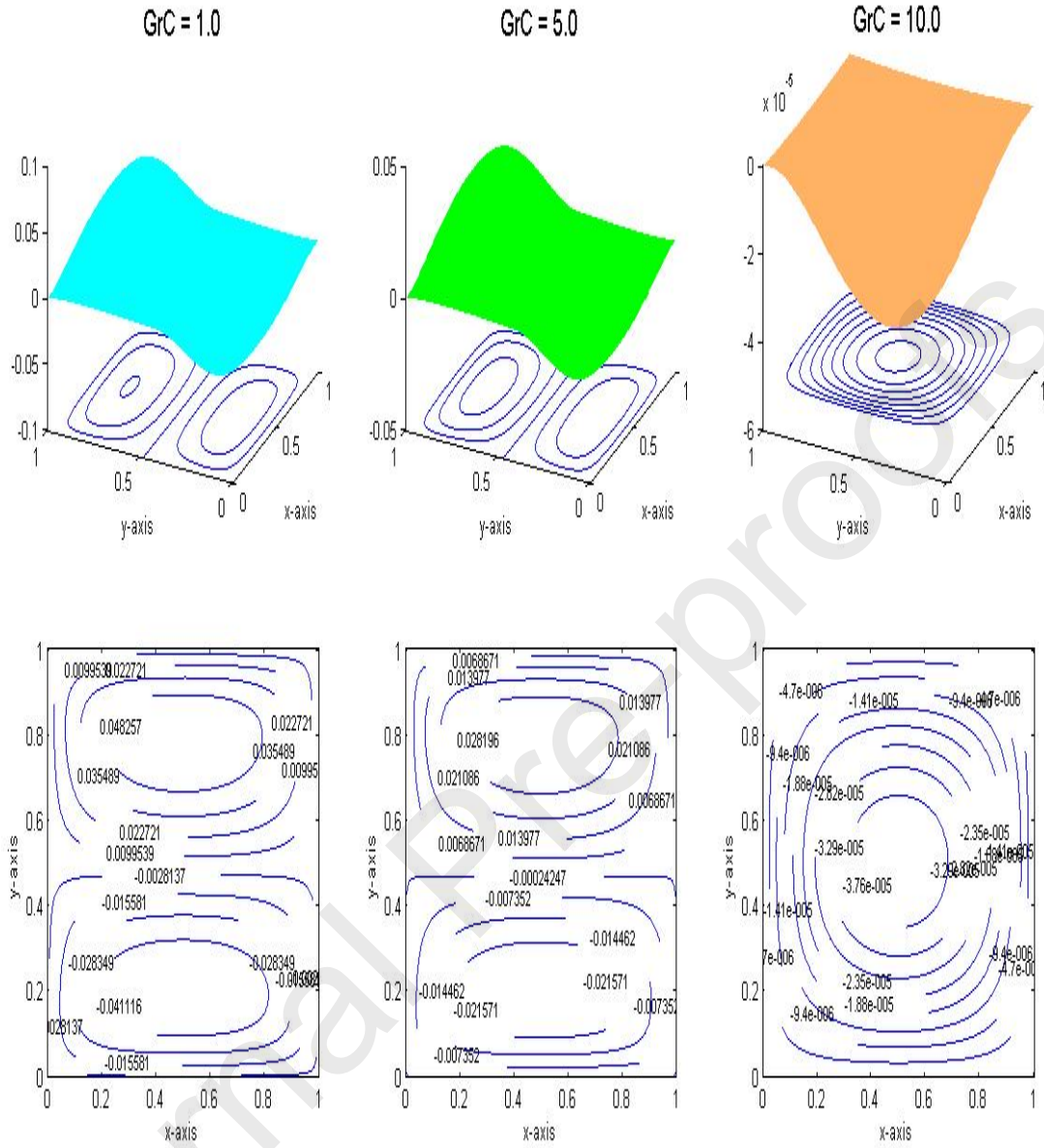


Figure 3b. Profiles of velocity, temperature and concentration for distinct GrT .



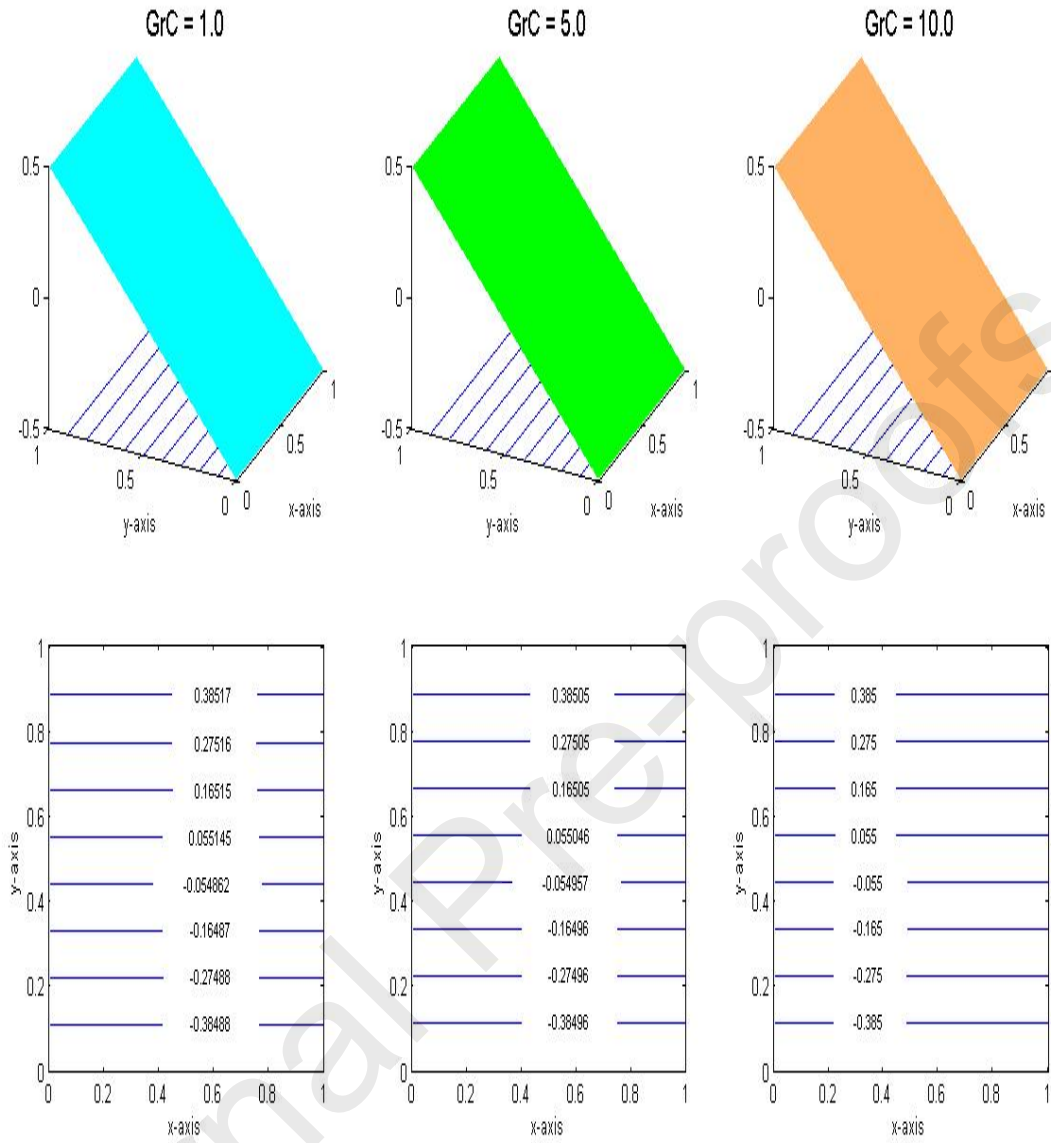
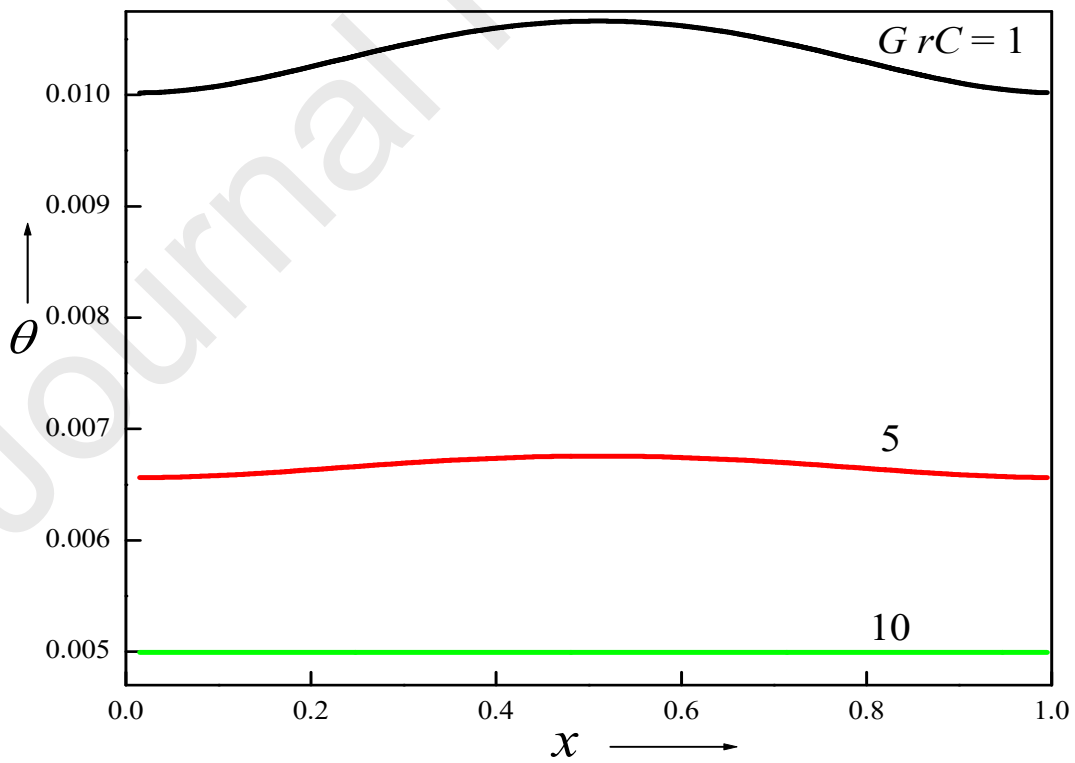
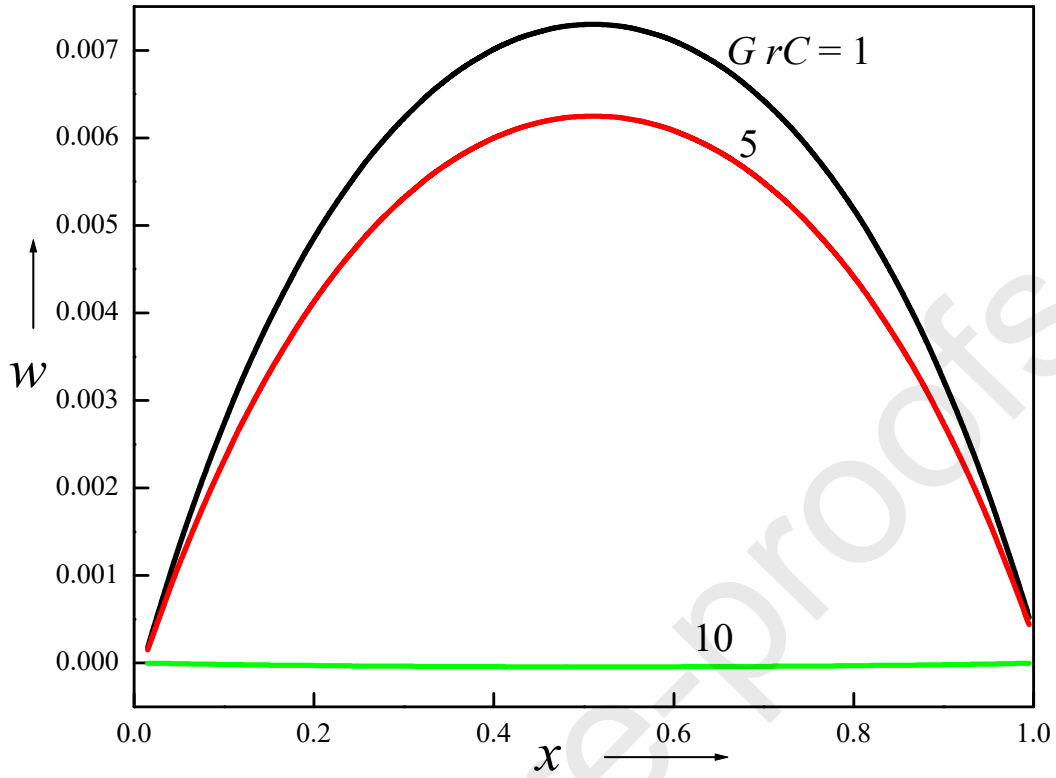


Figure 4a. Isocontours of velocity and temperature for distinct GrC .



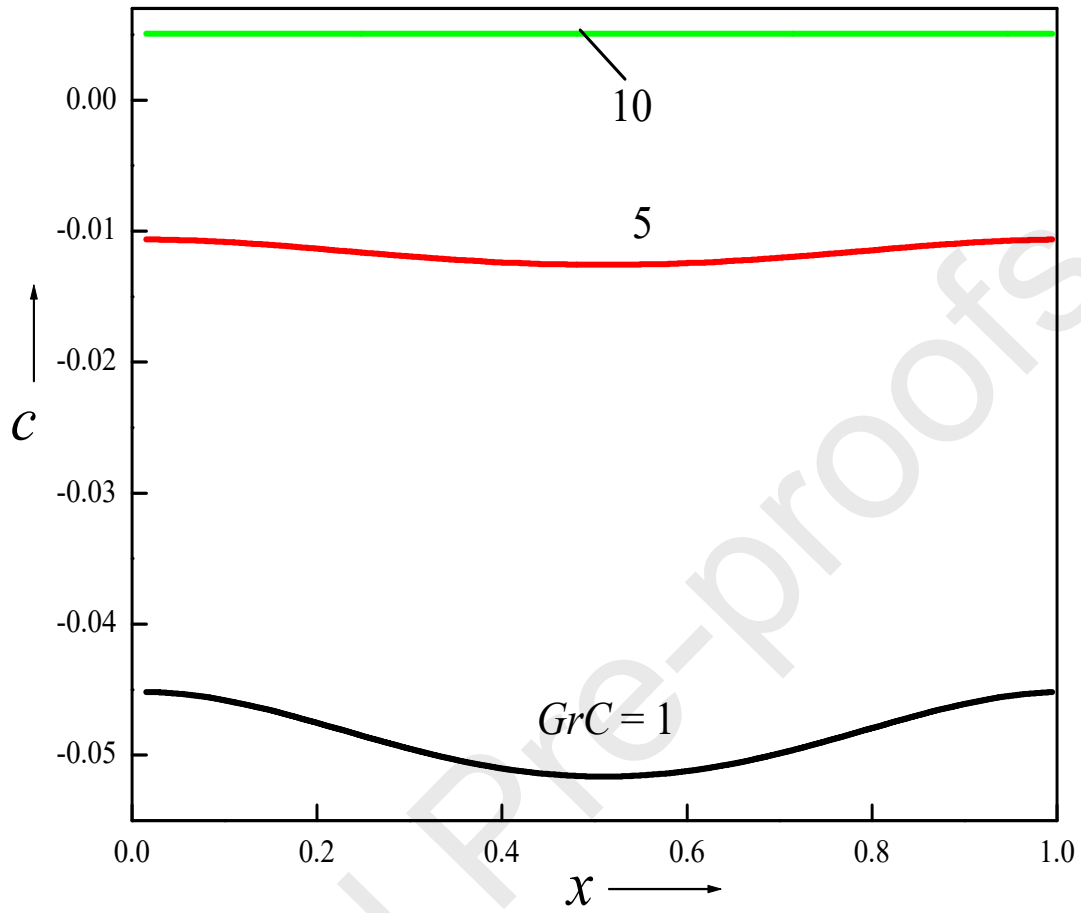


Figure 4b. Profiles of velocity, temperature and concentration for distinct GrC .

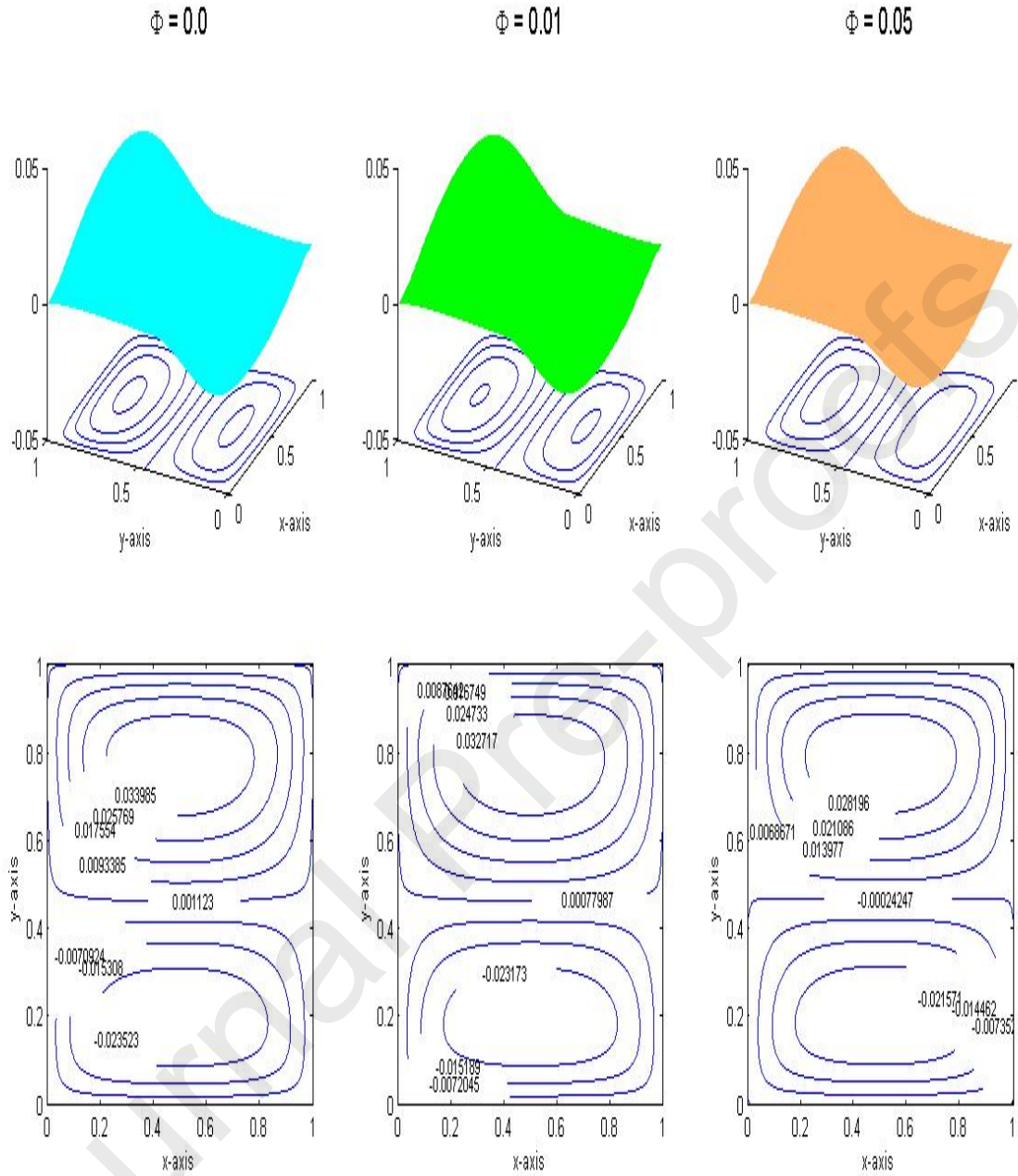
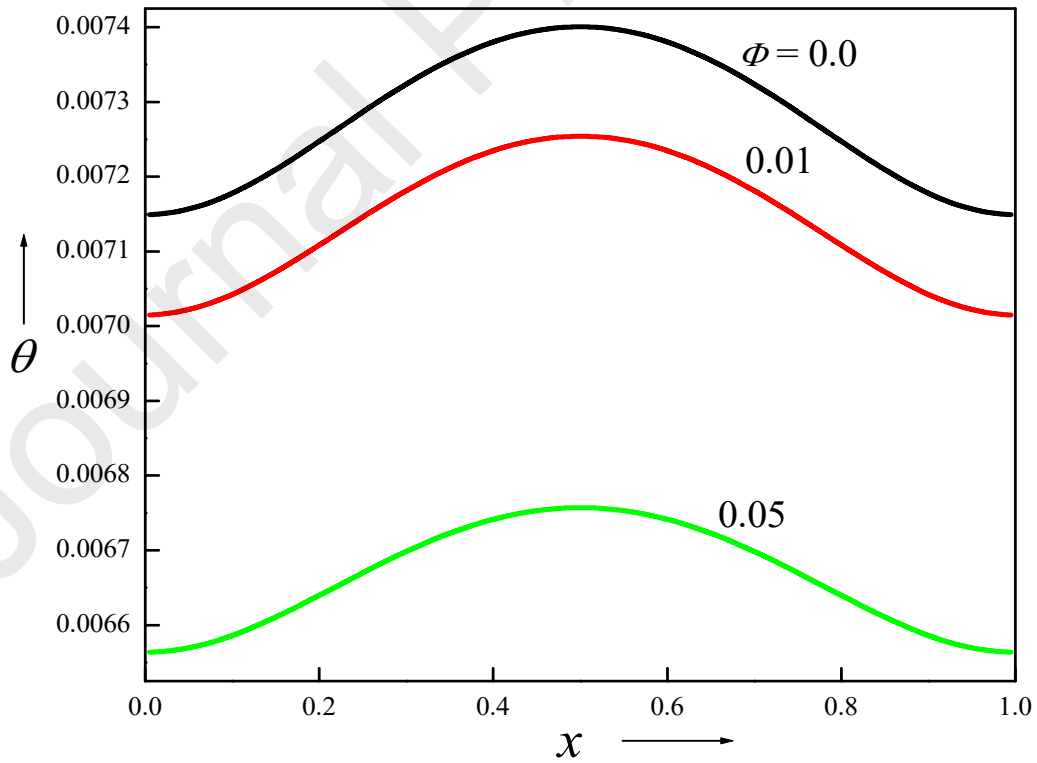
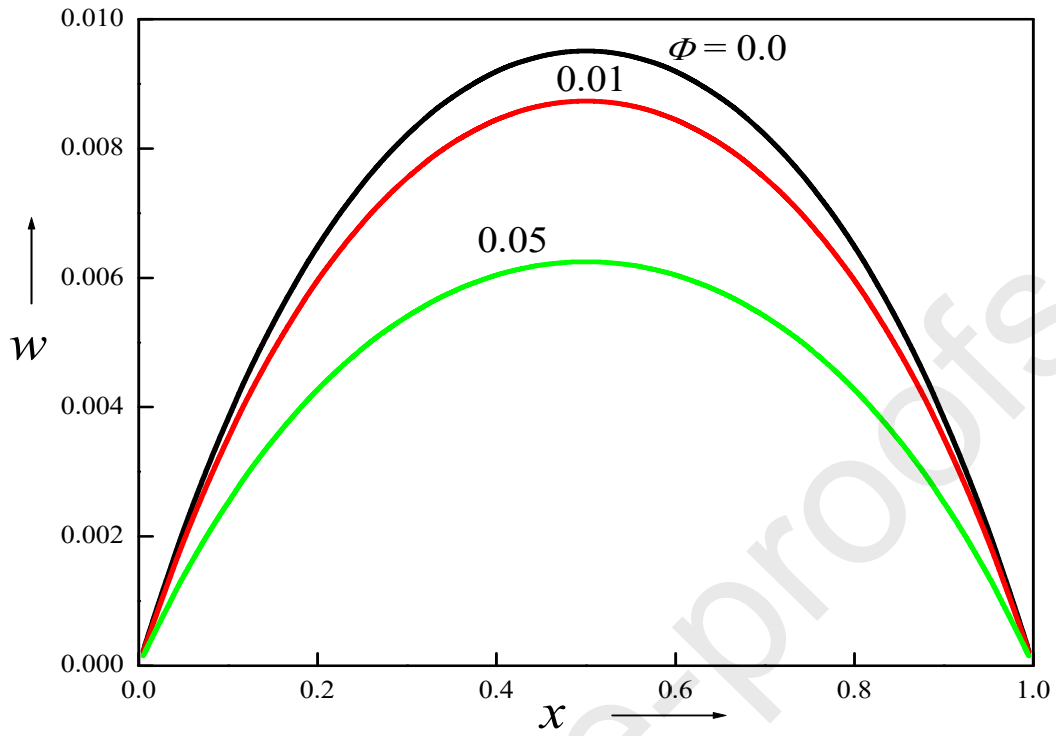


Figure 5a. Isocontours of velocity for distinct Φ .



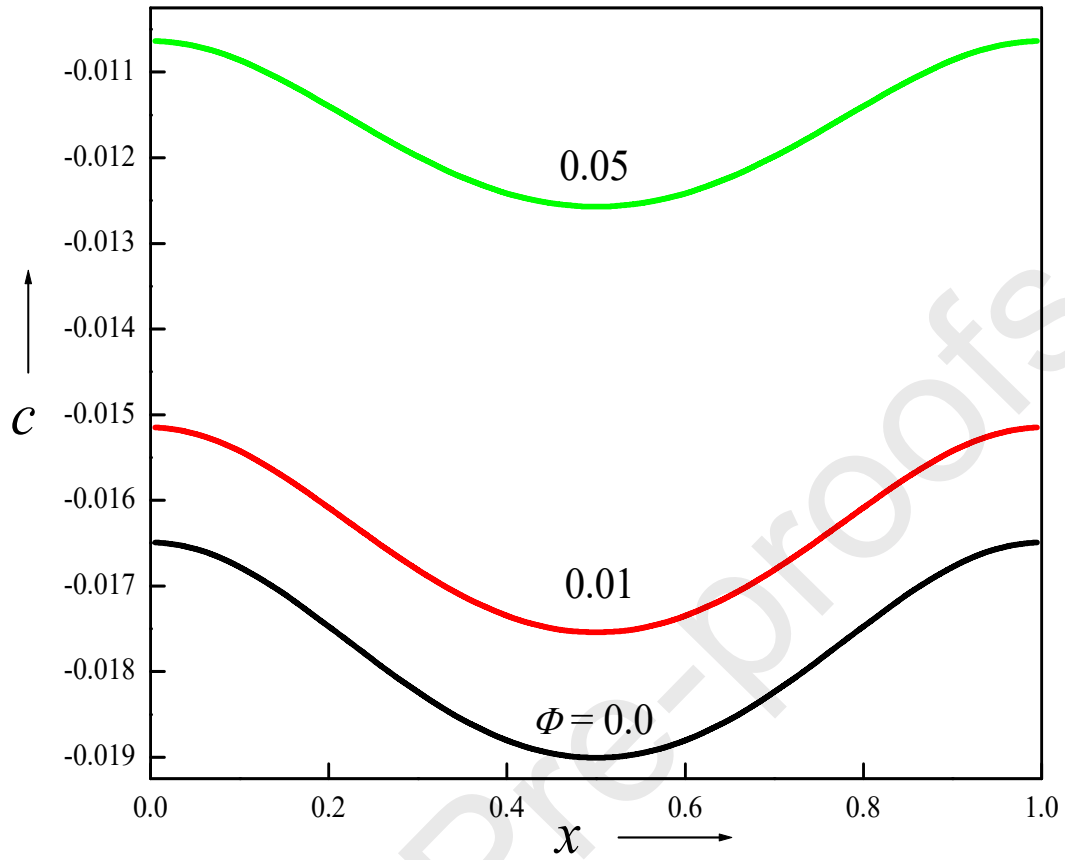


Figure 5b. Profiles of velocity, temperature and concentration for distinct Φ .

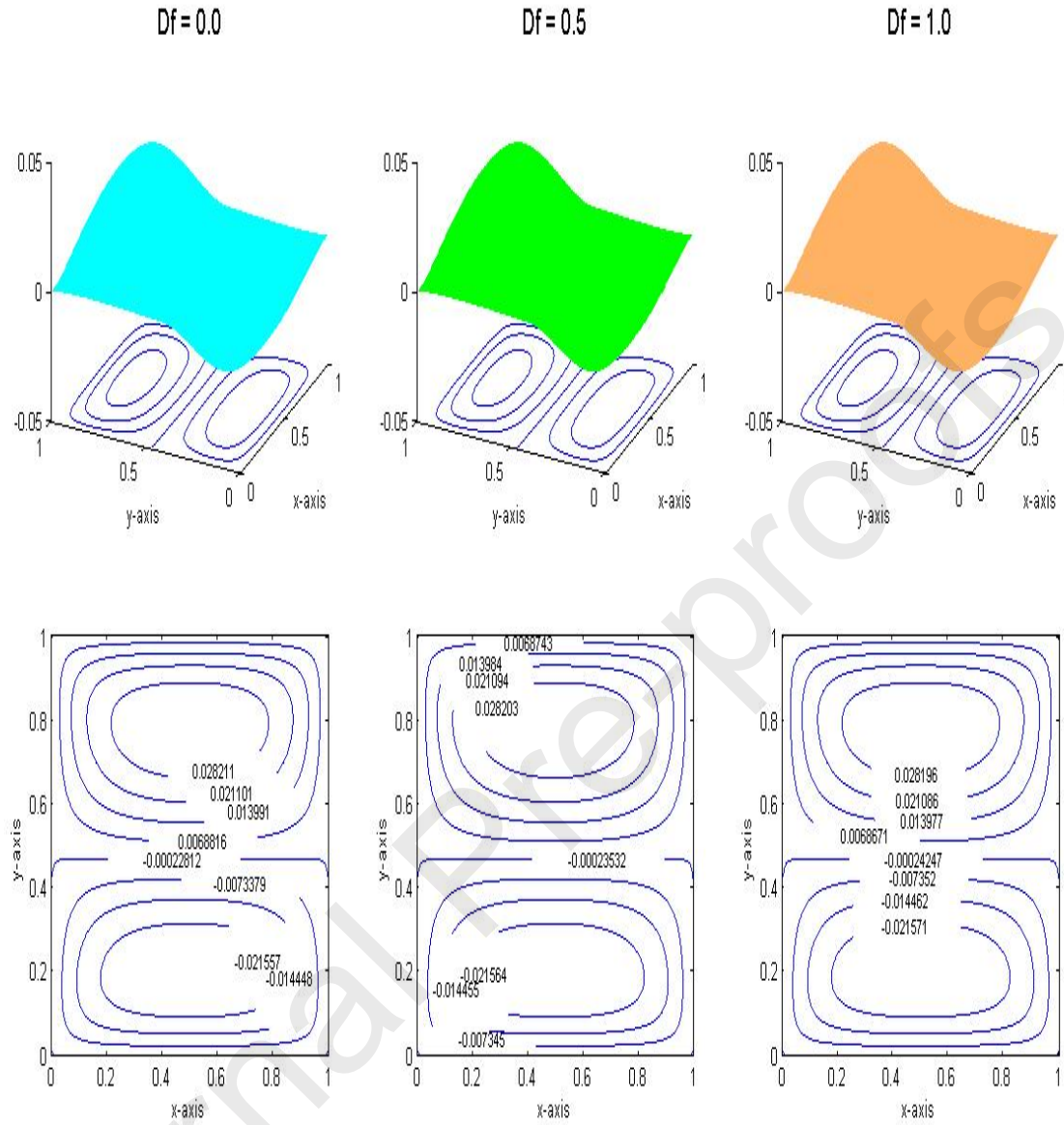
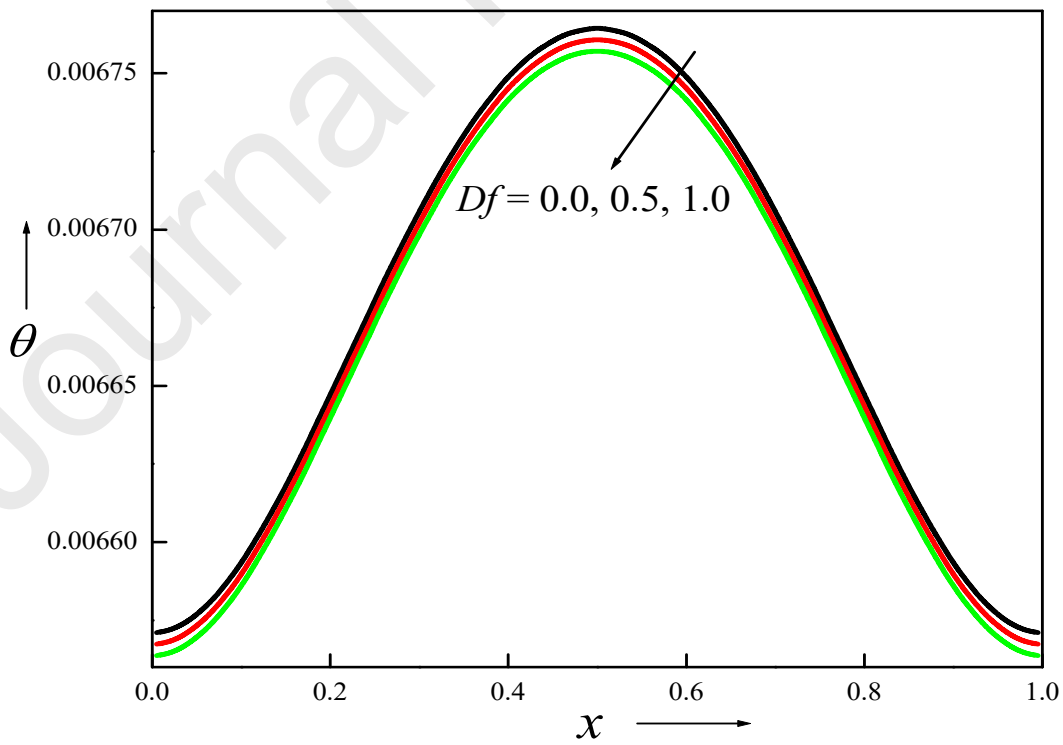
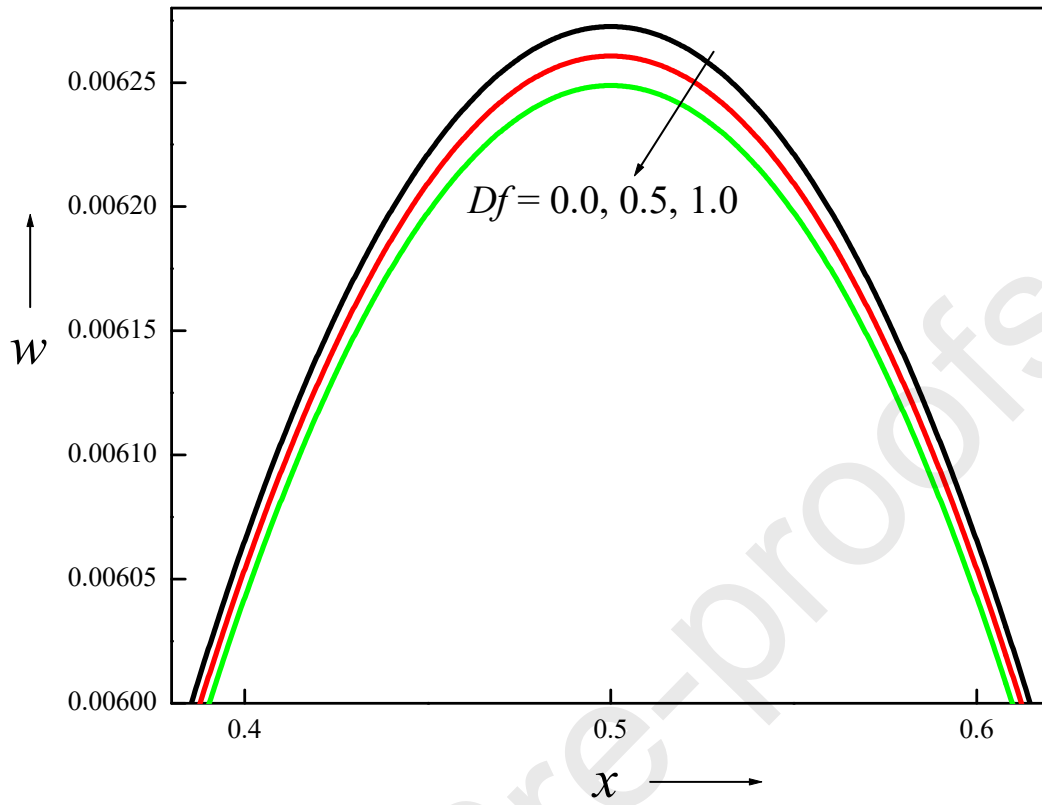


Figure 6a. Isocontours of velocity for distinct Df .



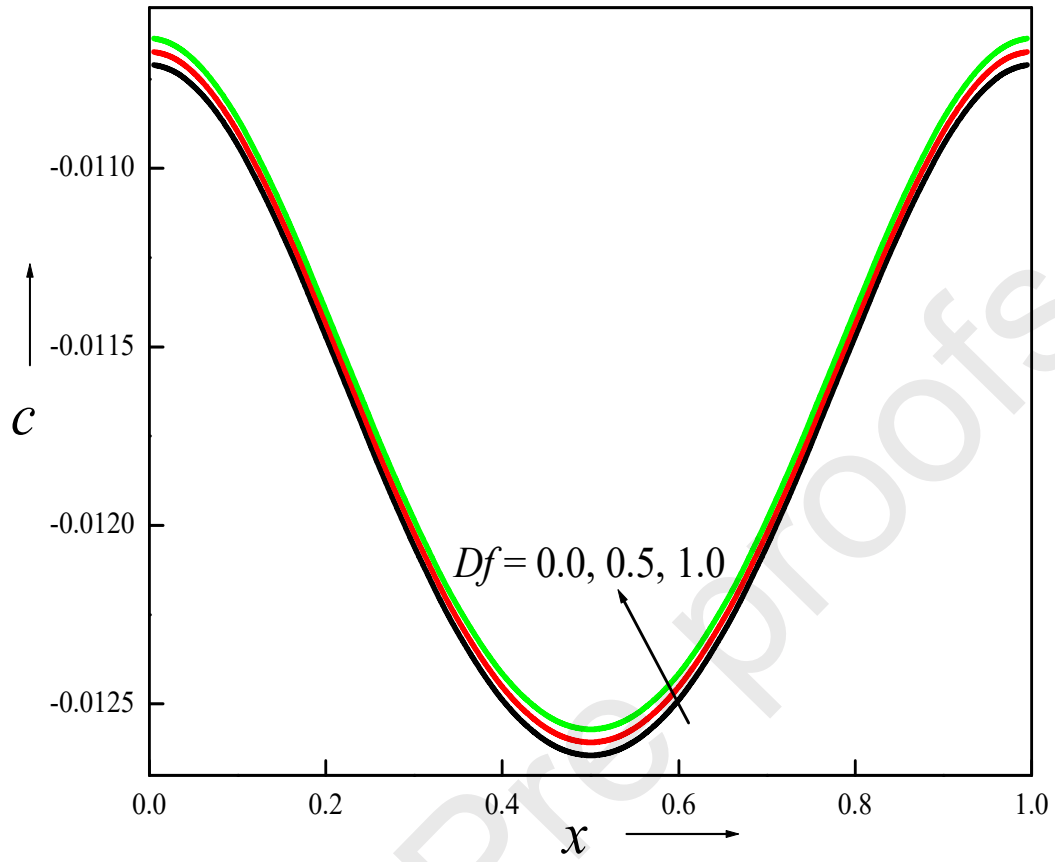


Figure 6b. Profiles of velocity, temperature and concentration for distinct Df .

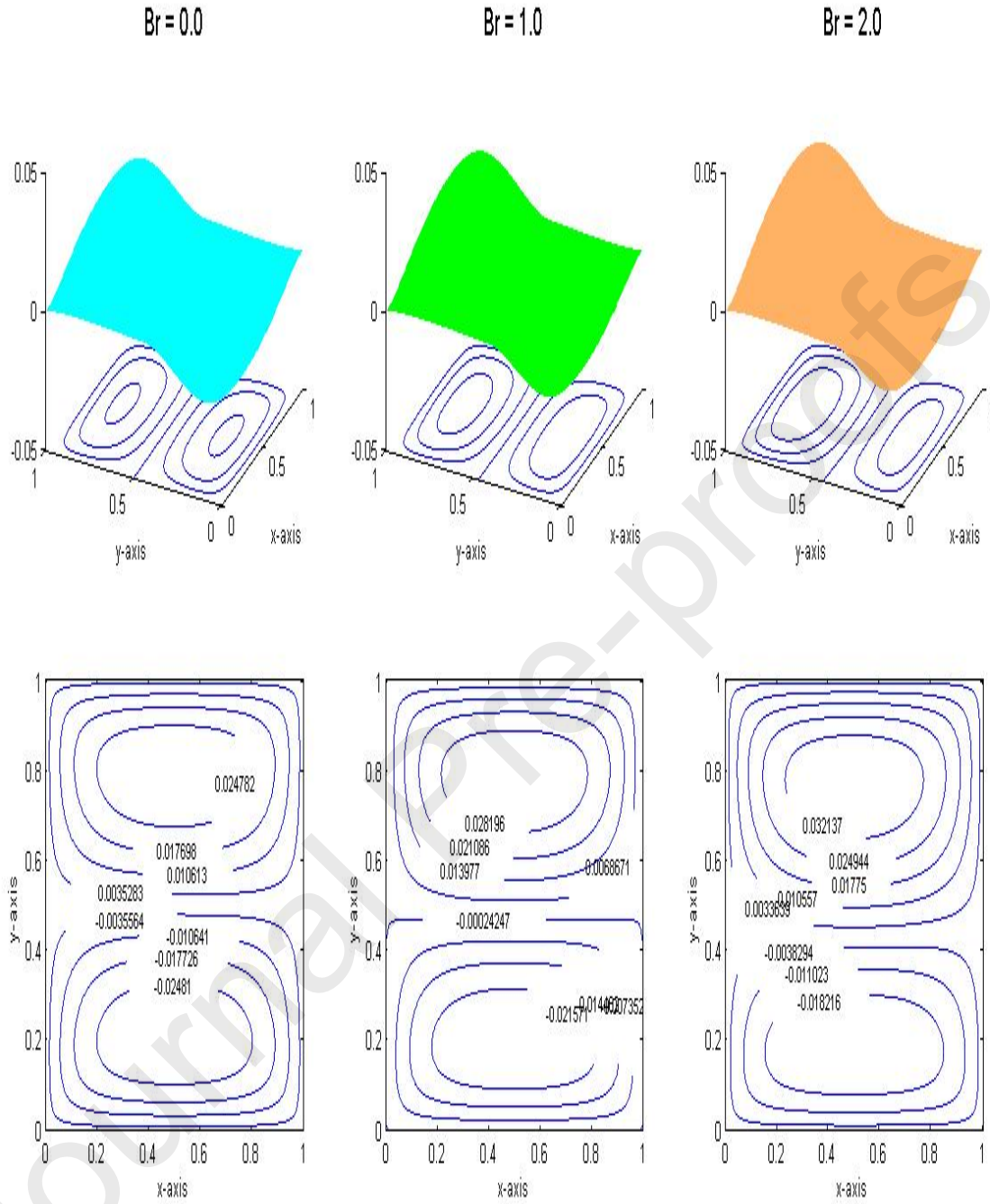
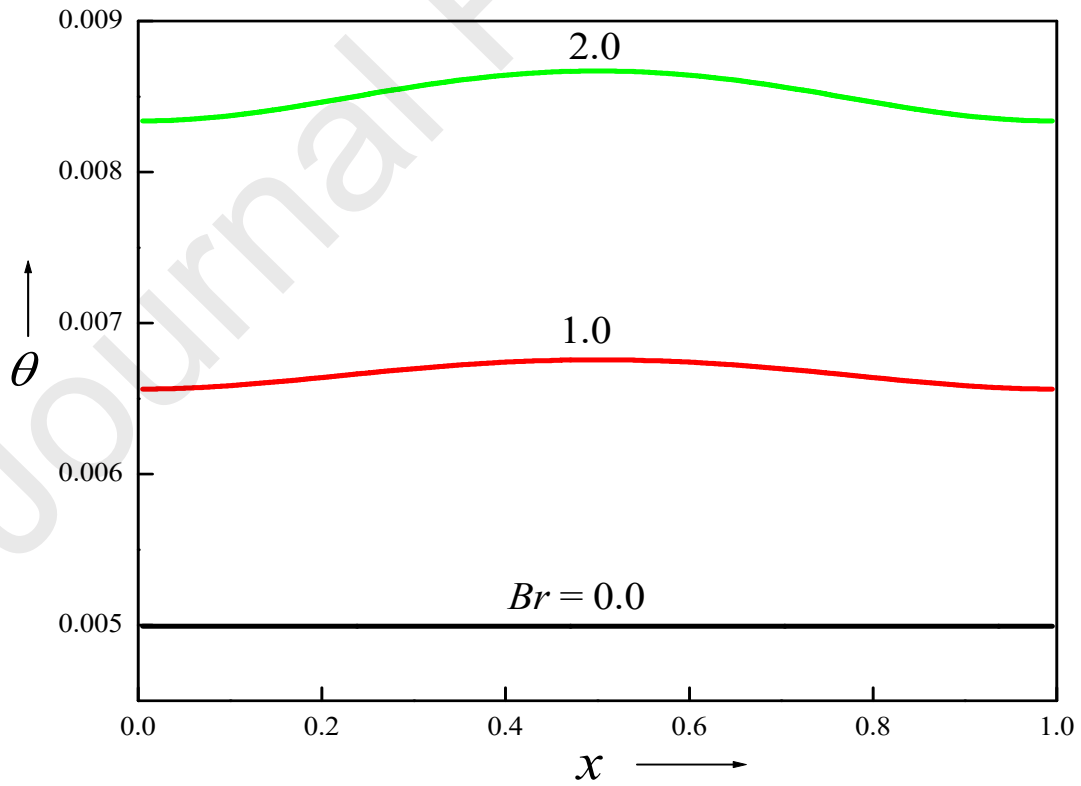
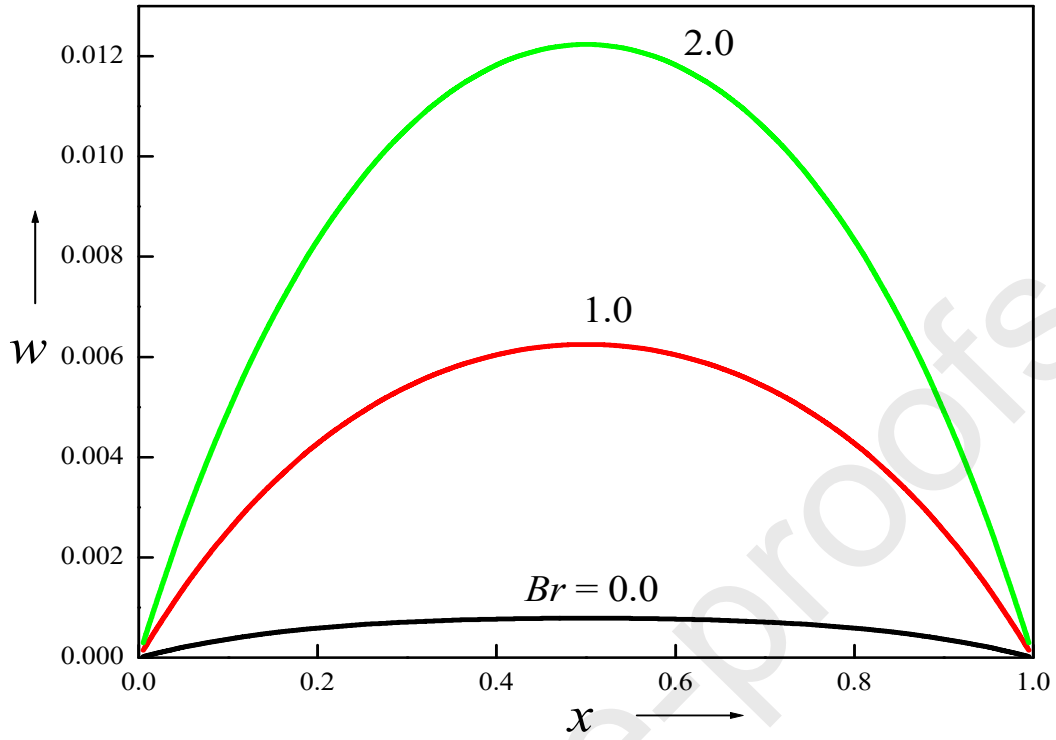


Figure 7a. Isocontours of velocity for distinct Br .



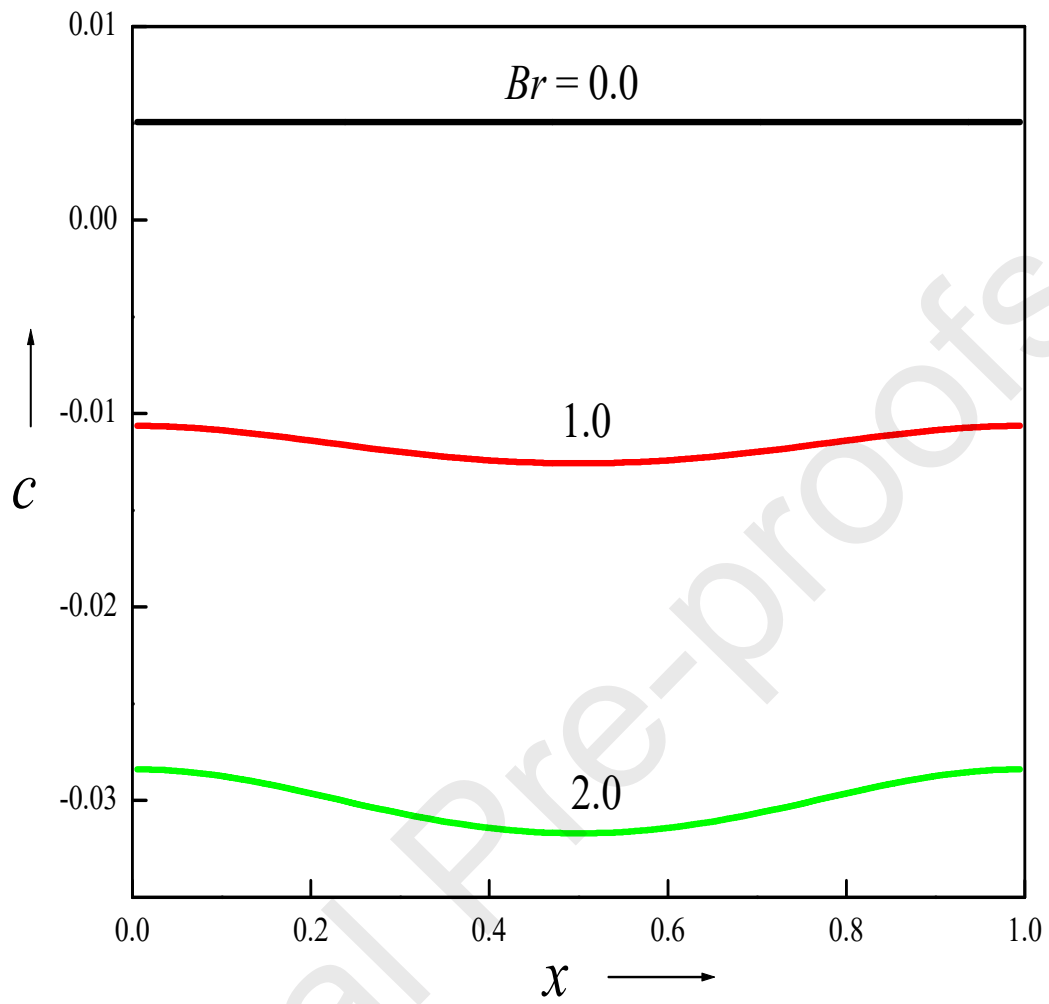


Figure 7b. Profiles of velocity, temperature and concentration for distinct Br .

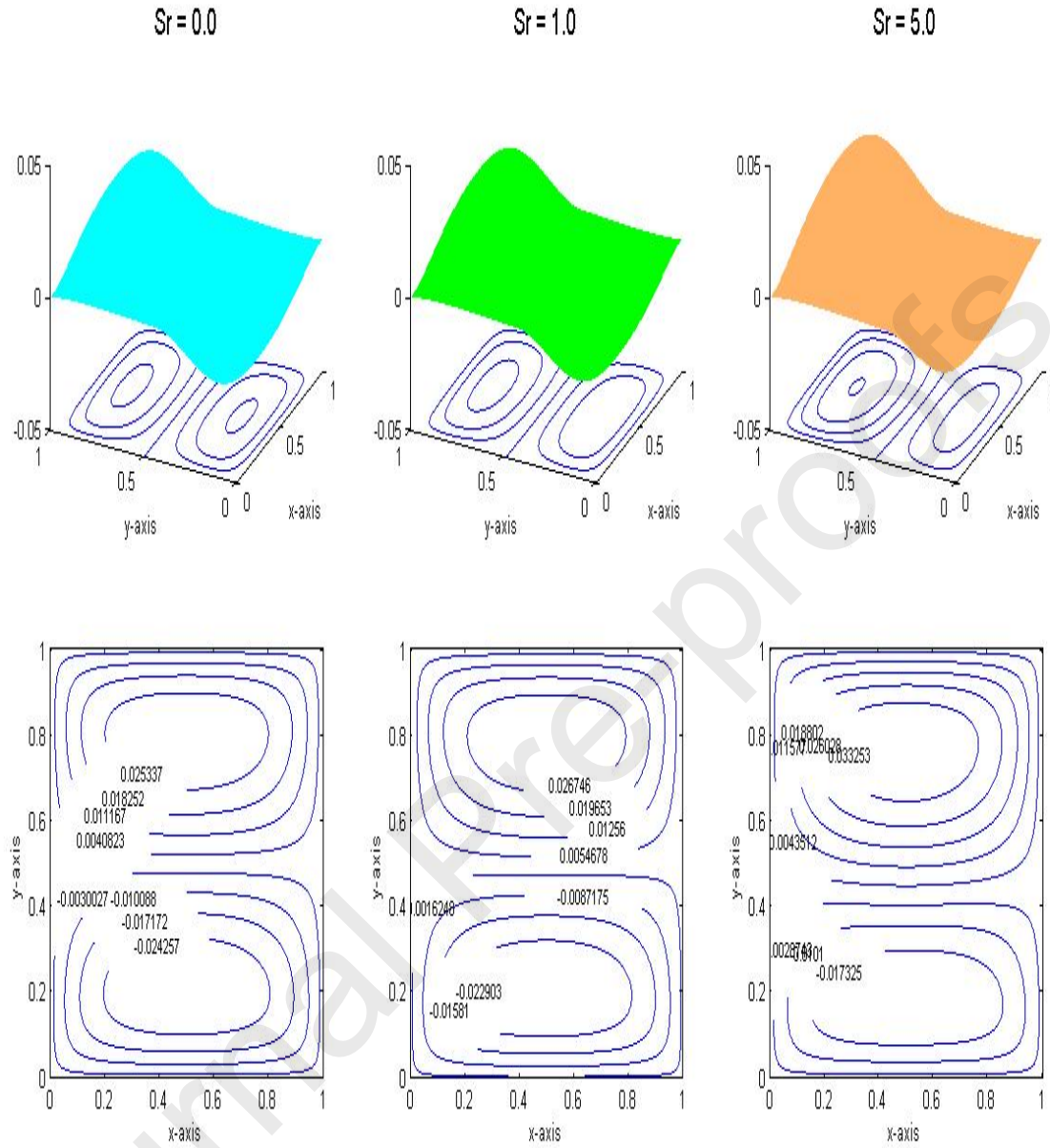
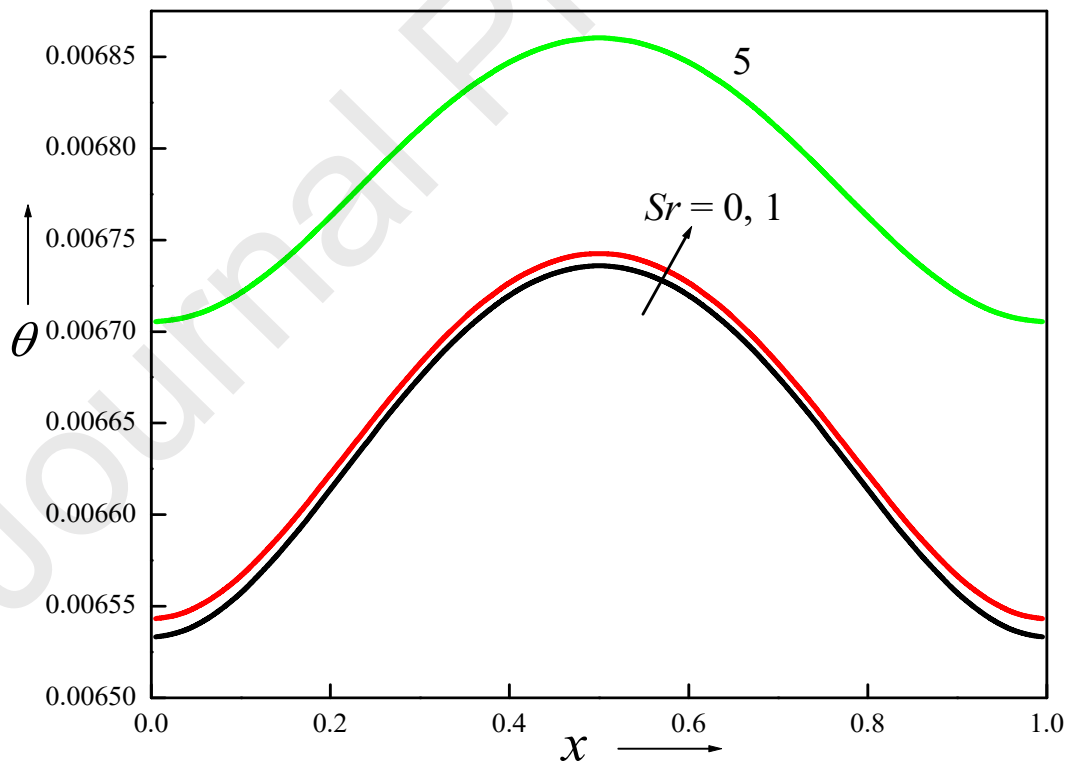
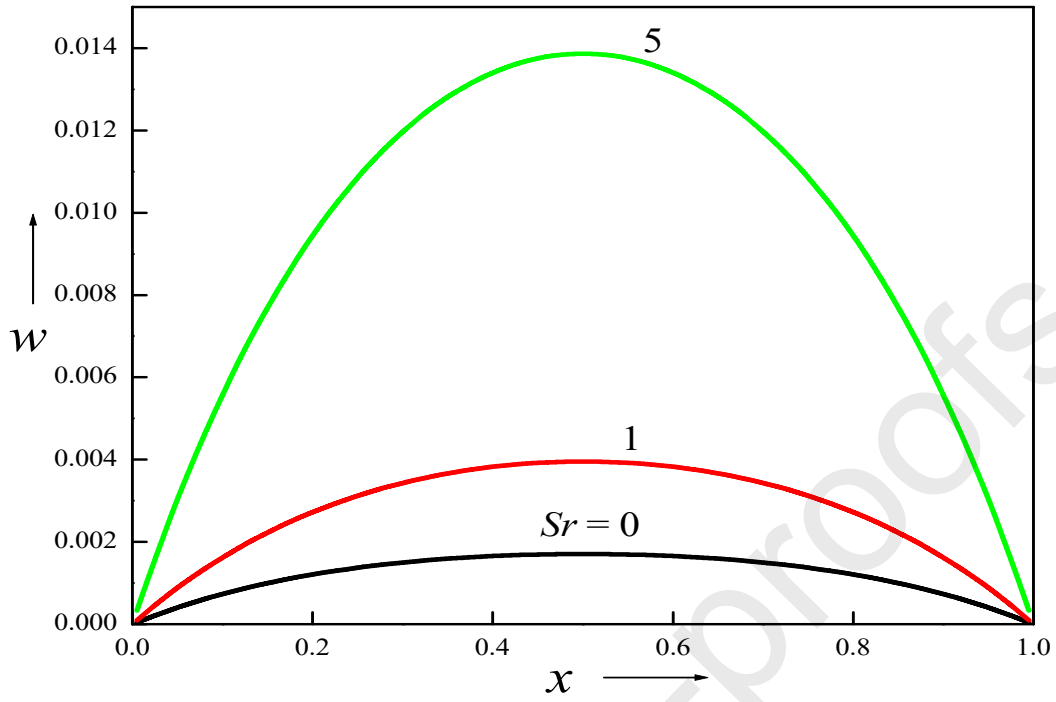


Figure 8a. Isocontours of velocity for distinct Sr .



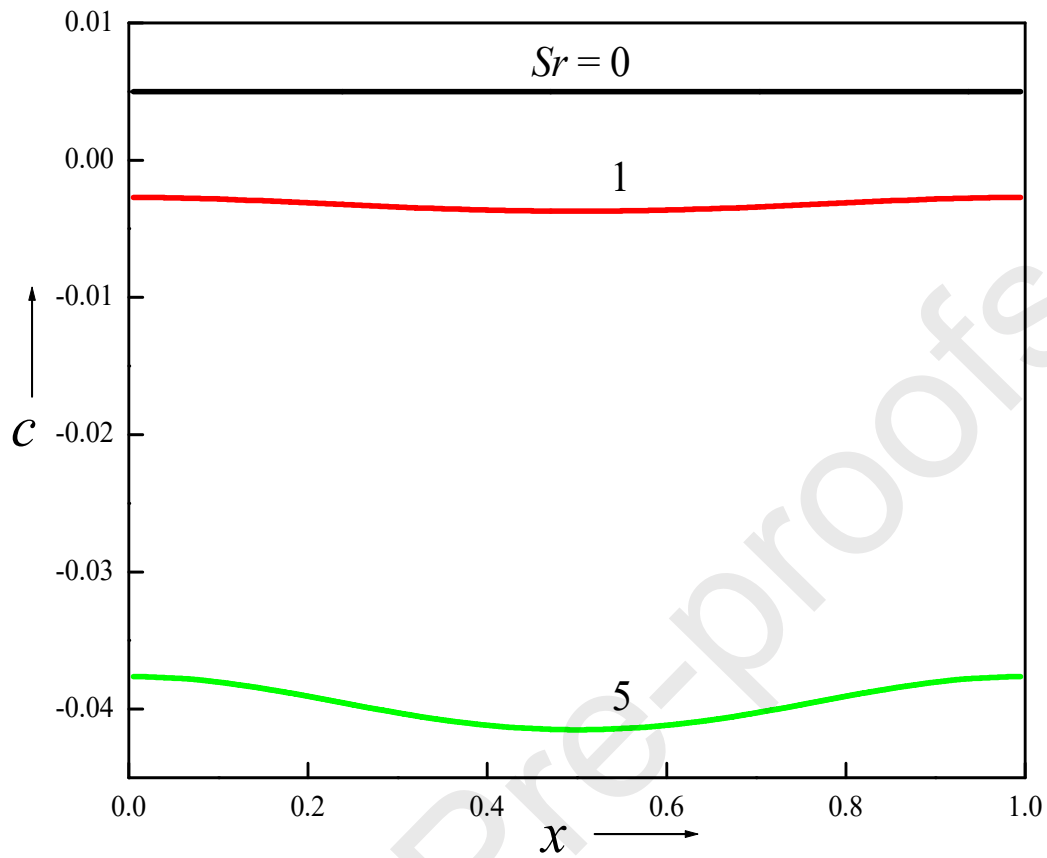


Figure 8b. Profiles of velocity, temperature and concentration for distinct Sr .

Table 1. Thermophysical properties for pure water and various types of nanoparticles.

Property	Pure water	Ag	Cu	Diamond	SiO ₂	TiO ₂
ρ (kg/m ³)	997.1	10500	8933	3510	2200	4250
μ (kg/m·s)	1×10^{-3}	–	–	–	–	–
k (W/mK)	0.613	429	400	1000	1.2	8.9538
C_p (J/kg·K)	4179	235	385	497.26	703	686.2
β (1/K)	207×10^{-6}	18×10^{-6}	17×10^{-6}	1.0×10^{-6}	5.5×10^{-6}	0.17×10^{-6}

Table 2. Values of heat transport rate for different grids.

Grids	$d\theta/dy _{y=0}$	$d\theta/dy _{y=1}$	$dw/dy _{y=0}$	$dw/dy _{y=1}$
10 × 10	0.583219116325	0.573103647205	-0.13011774044	-0.14335669948
50 × 50	0.583403900208	0.572944998828	-0.13278021128	-0.14511004150
100 × 100	0.583419236338	0.572949050341	-0.13287818323	-0.14515010952
150 × 150	0.583429603306	0.572957730781	-0.13290713985	-0.14514607580
200 × 200	0.583439231189	0.572967098217	-0.13292589167	-0.14513553302

Table 3. Values of flow rate and skin friction.

	Q	$dw/dy _{y=0}$	$dw/dy _{y=1}$	$dw/dx _{x=0}$	$dw/dx _{x=1}$
Nanoparticles					
copper	0.0023025	-0.13310415	-0.1449015	0.00796914	-0.0079691
diamond	0.0020508	-0.12873015	-0.1392388	0.00709708	-0.0070970
silver	0.0023692	-0.13420577	-0.1463445	0.00820014	-0.0082001
TiO ₂	0.0020980	-0.12845778	-0.1392080	0.00726051	-0.0072605
SiO ₂	0.0023095	-0.12832593	-0.1401598	0.00799377	-0.00799377
GrT					
1	0.0012114	0.11426126	0.1080502	0.00419064	-0.0041906
10	0.0023025	-0.13310415	-0.1449015	0.00796914	-0.0079691
20	0.0031687	-0.34192706	-0.5039821	0.11106165	-0.1110616
GrC					
1	0.0025414	-0.24356079	-0.2565736	0.00879172	-0.00879172
10	-0.0001874	-0.00046053	0.0004779	-0.00064958	0.00064958
15	0.0067998	0.15733330	0.1225119	0.02366885	-0.023668857
Φ					
0	0.0036513	-0.1509102	-0.1696142	0.01264640	-0.012646409
0.01	0.0033297	-0.1473131	-0.1643701	0.01153020	-0.011530201
0.05	0.0023025	-0.1331041	-0.1449015	0.00796914	-0.007969147
Df					
0	0.0024078	-0.1328530	-0.1451777	0.00833446	-0.00833446

0.5	0.0023551	-0.1329786	-0.1450396	0.00815175	-0.00815175
1.0	0.0023025	-0.1331041	-0.1449015	0.00796914	-0.00796914
<i>Br</i>					
0	0.0001024	-0.1391326	-0.1386198	-0.00035496	0.00035496
1.0	0.0023025	-0.1331041	-0.1449015	0.00796914	-0.00796914
2.0	0.0049383	-0.1267846	-0.1520682	0.01713902	-0.01713902
<i>Sr</i>					
0	0.0003784	-0.1379139	-0.1398533	0.00130889	-0.00130889
1	0.0013305	-0.1355121	-0.1423296	0.00460245	-0.00460245
5	0.0055245	-0.1254103	-0.1537053	0.01919024	-0.01919024
<i>Sc</i>					
0	0.0003784	-0.1379139	-0.1398533	0.00130889	-0.00130889
1	0.0007578	-0.1369516	-0.1408349	2.62102296	-2.62102296
5	0.0023025	-0.1331041	-0.1449015	0.00796914	-0.00796914
<i>A</i>					
0.5	0.0005617	-0.101012	-0.1040866	0.0035618	-0.00356185
1.0	0.00230259	-0.1331041	-0.1449015	0.0079691	-0.00796914
2.0	0.00470704	-0.148118	-0.1718424	0.0100337	-0.0100337

Table 4. Values of heat transport strength.

	$d\theta/dy _{y=0}$	$d\theta/dy _{y=1}$
Nanoparticles		
copper	0.583583055751323	0.573122204411961
diamond	0.583488018931189	0.573781668776581
silver	0.583692147547072	0.573035121095960
TiO ₂	0.568753149712701	0.559065091264544
SiO ₂	0.523049405534830	0.513285768604096
<i>GrT</i>		
1	0.582224049943819	0.575568793471494
10	0.583583055751323	0.573122204411961
20	0.619419791662531	0.505795389838861

<i>GrC</i>		
1	0.594815155669496	0.561150301411051
10	0.578733015254236	0.578732433739301
15	0.585543041278968	0.574218187802977
Φ		
0	0.505718851766624	0.493388710545642
0.01	0.520656680221904	0.508725080773597
0.05	0.583583055751323	0.573122204411961
<i>Df</i>		
0	0.583401028112696	0.572929784139775
0.5	0.583492057104163	0.573026061410841
1.0	0.583583055751323	0.573122204411961
<i>Br</i>		
0	0.578732726117073	0.578732726181541
1.0	0.583583055751323	0.573122204411961
2.0	0.587950068447393	0.566224716971227
<i>Sr</i>		
0	0.583845405982826	0.573494371235407
1	0.583705892605994	0.573320228244316
5	0.583311753463899	0.572320474757525
<i>Sc</i>		
0	0.583845405982826	0.573494371235407
1	0.583787513544375	0.573427323734631
5	0.583583055751323	0.573122204411961
<i>A</i>		
0.5	0.581895434162965	0.575350470245329
1.0	0.583583055751323	0.573122204411961
2.0	0.584444824336413	0.571589103395047

Table 5. Values of Sherwood number.

	$dc/dy _{y=0}$	$dc/dy _{y=1}$
Nanoparticles		
copper	0.456647248656081	0.547050427595054
diamond	0.459456500771577	0.543306174845028
silver	0.455928206921557	0.548022655639408
TiO ₂	0.458542782203340	0.544418231422072
SiO ₂	0.454858326649783	0.549034767853464
<i>GrT</i>		
1	0.468391841911601	0.525906887722200
10	0.456647248656081	0.547050427595054
20	0.146944458523644	1.12889198751162
<i>GrC</i>		
1	0.359578902581948	0.650512187384912
10	0.498561530907182	0.498566557013959
15	0.439708959769659	0.537578886549701
Φ		
0	0.442811482327280	0.566112894551605
0.01	0.445879328996851	0.561701800331132
0.05	0.456647248656081	0.547050427595054
<i>Df</i>		
0	0.458220340239399	0.548713332812226
0.5	0.457433663329219	0.547881300020034
1.0	0.456647248656081	0.547050427595054
<i>Br</i>		
0	0.498564029647737	0.498564029710819
1.0	0.456647248656081	0.547050427595054
2.0	0.418907315559963	0.606658844774543
<i>Sr</i>		
0	0.499999999978045	0.500000000021579
1	0.477792843280964	0.522669548121931

5	0.397479640150554	0.634947534215382
Sc		
0	0.499999999978045	0.500000000021579
1	0.490976062865653	0.508882714409585
5	0.456647248656081	0.547050427595054
A		
0.5	0.471231755208294	0.527793647549612
1.0	0.456647248656081	0.547050427595054
2.0	0.449199803246107	0.560299560072624

Table 6. Values of heat transport strength for $\Phi = 0.05$, $Br = 1$

GrT	$d\theta/dy _{y=0}$	$d\theta/dy _{y=0}$	$d\theta/dy _{y=1}$	$d\theta/dy _{y=1}$
	Present data	Umavathi et al. [32]	Present data	Umavathi et al. [32]
1	0.5787734740818	0.5787734740818	0.5783595511908	0.5783595511908
10	0.5987622094064	0.5987622094064	0.5573164661297	0.5573164661297
20	0.6544708408270	0.6544708408270	0.4853216080781	0.4853216080781

References

1. O. Manca, S. Nardini, K. Khanafer, K. Vafai, Effect of heat wall position on mixed convection in a channel with an open cavity, *Numerical Heat Transfer* 43 (2003) 259–282.
2. H.K. Wee, R.B. Keey, M.J. Cunningham, Heat and moisture transfer by natural convection in a rectangular cavity, *Int. J. Heat Mass Transfer* 32 (1989) 765–778.
3. C. Beghein, F. Haghighat, F. Allard, Numerical study of double-diffusive natural convection in a square cavity, *Int. J. Heat Mass Transfer* 35 (1992) 833–846.
4. K. Ghorayeb, H. Khallouf, A. Mojtabi, Onset of oscillatory flows in double diffusive convection, *Int. J. Heat Mass Transfer* 42 (1999) 629–643.
5. M. Mamou, P. Vasseur, E. Bilgen, Multiple solutions for double-diffusive convection in a vertical porous enclosure, *Int. J. Heat Mass Transfer* 38 (1995) 1787–1798.
6. O.V. Trevisan, A. Bejan, Natural convection with combined heat and mass transfer buoyancy effects in a porous medium, *Int. J. Heat Mass Transfer* 28 (1985) 1597–1611.

7. B. Goyeau, J.P. Songbe, D. Gobin, Numerical study of double-diffusive natural convection in a porous cavity using the Darcy-Brinkman formulation, *Int. J. Heat Mass Transfer* 39 (1996) 1363–1378.
8. R. Bennacer, A. Tobbal, H. Beji, P. Vasseur, Double-diffusive convection in a vertical enclosure filled with anisotropic porous media, *Int. J. Thermal Sciences* 40 (2001) 30–41.
9. S.K. Das, S.U. Choi, W. Yu, T. Pradeep, *Nanofluids: science and technology*, John Wiley & Sons, 2007.
10. D.A. Nield, A. Bejan, *Convection in porous media*, Springer, 2006.
11. E.E.S. Michaelides, *Nanofluidics: thermodynamic and transport properties*, Springer, 2014.
12. A. Shenoy, M. Sheremet, I. Pop, *Convective flow and heat transfer from wavy surfaces: Viscous Fluids, Porous Media, and Nanofluids*, CRC Press, 2016.
13. J. Buongiorno, D.C. Venerus, N. Prabhat, T. McKrell, J. Townsend, R. Christianson, Y.V. Tolmachev, P. Keblinski, L.-w. Hu, J.L. Alvarado, A benchmark study on the thermal conductivity of nanofluids, *Journal of Applied Physics* 106 (2009) 94312.
14. S. Kakaç, A. Pramuanjaroenkij, Review of convective heat transfer enhancement with nanofluids, *Int. J. Heat Mass Transfer* 52 (2009) 3187–3196.
15. K.V. Wong, O. de Leon, Applications of nanofluids: current and future, *Advances in Mechanical Engineering* 2 (2010) 519659.
16. O. Manca, Y. Jaluria, D. Poulikakos, *Heat transfer in nanofluids*, SAGE Publications Sage UK: London, England, 2010.
17. T.G. Myers, H. Ribera, V. Cregan, Does mathematics contribute to the nanofluid debate?, *Int. J. Heat Mass Transfer* 111 (2017) 279–288.
18. R. Ahmad, M. Mustafa, M. Turkyilmazoglu, Buoyancy effects on nanofluid flow past a convectively heated vertical Riga-plate: A numerical study, *Int. J. Heat and Mass Transfer* 111 (2017) 827–835.
19. R.K. Tiwari, M.K. Das, Heat transfer augmentation in a two-sided lid-driven differentially heated square cavity utilizing nanofluids, *Int. J. Heat Mass Transfer* 50 (2007) 2002–2018.
20. A.I. Alsabery, T. Tayebi, A.J. Chamkha, I. Hashim, Effects of non-homogeneous nanofluid model on natural convection in a square cavity in the presence of conducting solid block and corner heater, *Energies* 11 (2018) 2507.
21. M. Turkyilmazoglu, Free and circular jets cooled by single phase nanofluids, *European J. of Mechanics/B Fluids* 76 (2019) 1–6.
22. M. Turkyilmazoglu, Fully developed slip flow in a concentric annuli via single and dual phase nanofluids models, *Computer Methods and Programs in Biomedicine* 179 (2019) 104997.

23. M. Turkyilmazoglu, Single phase nanofluids in fluid mechanics and their hydrodynamic linear stability analysis, *Computer Methods and Progress in Biomedicine* 187 (2020) 105171.
24. J.C. Umavathi, M.B. Mohite, Double diffusive convective transport in a nanofluid-saturated porous layer with cross diffusion and variation of viscosity and conductivity, *Heat Transfer – Asian Research* 43 (2014) 628–652.
25. J.C. Umavathi, M.B. Mohite, Convective transport in a porous medium layer saturated with a Maxwell nanofluid, *J. King Saud University – Engineering Sciences* 28(1) (2016) 56–68.
26. J.C. Umavathi, Rayleigh-Benard convection subject to time dependent wall temperature in a porous medium layer saturated by a nanofluid, *Meccanica* 50 (2015) 981–994.
27. J.C. Umavathi, A.J. Chamkha, Stability analysis of cross diffusion for the Walters B fluid model saturated with permeable fluid, *J. Thermal Science and Engineering Applications* 11 (2019) 041014-1.
28. J.C. Umavathi, O. Anwar Bég, Modeling the onset of thermosolutal convective instability in a non-Newtonian nanofluid-saturated porous medium layer, *Chinese J. Physics* 68 (2020) 147–167.
29. F. Talebi, A.H. Mahmoudi, M. Shahi, Numerical study of mixed convection flows in a square lid-driven cavity utilizing nanofluid, *Int. Commun. Heat Mass Transfer* 37 (2010) 79–90.
30. M. Benzema, Y.K. Benkahla, A. Boudiaf, S.-E. Ouyahia, M. El Ganaoui, Magnetic field impact on nanofluid convective flow in a vented trapezoidal cavity using Buongiorno’s mathematical model, *Eur. Phys. J. Appl. Phys.* 88 (2019) 11101.
31. S. Lahlou, N. Labsi, Y.K. Benkahla, A. Boudiaf, S.-E. Ouyahia, Flow of viscoplastic fluids containing hybrid nanoparticles: Extended Buongiorno’s model, *Journal of Non-Newtonian Fluid Mechanics* 281 (2020) 104308.
32. J.C. Umavathi, I.C. Liu, M.A. Sheremet, Convective heat transfer in a vertical rectangular duct filled with a nanofluid, *Heat Transfer – Asian Research* 45 (2016) 661–679.
33. M. Shekar, J.C. Umavathi, Influence of viscous dissipation on non-Darcy mixed convection flow of nanofluid, *Heat Transfer – Asian Research* 46 (2017) 176–199.
34. J.C. Umavathi, O. Ojjela, K. Vajravelu, Numerical analysis of convective flow and heat transfer of nanofluids in a vertical rectangular duct using Darcy-Forchheimer-Brinkman model, *Int. J. Thermal Sciences* 11 (2017) 511–524.
35. J.C. Umavathi, M.A. Sheremet, Influence of temperature dependent conductivity of a nanofluid in a vertical rectangular duct, *Int. J. Nonlinear Mechanics* 78 (2016) 17–28.
36. J.C. Umavathi, M. Sasso, Free convection flow in a duct filled with nanofluid and saturated with porous medium: Variable properties, *Journal of Porous Medium* 9 (2018) 155–176.

37. D. Wen, Y. Ding, Experimental investigation into convective heat transfer of nanofluids at the entrance region under laminar flow conditions, *Int. J. Heat Mass Transfer* 47 (2004) 5181–5188.
38. J. Buongiorno, Convective transport in nanofluids, *J. Heat Transfer* 128 (2006) 240–250.
39. S.-E. Ouyahia, Y.K. Benkahla, W. Berabou, A. Boudiaf, Numerical study of the flow in a square cavity filled with Carbopol-TiO₂ nanofluid, *Powder Technology* 311 (2017) 101–111.
40. J.C. Umavathi, Effect of thermal modulation on the onset of convection in a porous medium layer saturated by nanofluids, *Trans. Porous Media* 98 (2013) 59–79.
41. M. Alinia, D. Ganji, M. Gorji-Bandpy, Numerical study of mixed convection in an inclined two sided lid driven cavity filled with nanofluid using two-phase mixture model, *Int. Commun. Heat Mass Transfer* 38 (2011) 1428–1435.
42. K. Khanafer, K. Vafai, M. Lightstone, Buoyancy-driven heat transfer enhancement in a two-dimensional enclosure utilizing nanofluids, *Int. J. Heat Mass Transfer* 46(19) (2003) 3639–3653.
43. R.Y. Jou, S.C. Tzeng, Numerical research of nature convective heat transfer enhancement filled with nanofluids in rectangular enclosures, *Int. Commun. Heat Mass Transfer* 33(6) (2006) 727–736.
44. S. Kherroubi, Y.K. Benkahla, N. Labsi, K. Ragui, A. Bensaci, A. Boutra, S.-E. Ouyahia, M. Benzema, Two- and three-dimensional comparative study of heat transfer and pressure drop characteristics of nanofluids flow through a ventilated cubic cavity (part I: Newtonian nanofluids), *Journal of Thermal Analysis and Calorimetry* (2020) <https://doi.org/10.1007/s10973-020-09588-w>
45. M. Benzema, Y.K. Benkahla, N. Labsil, E. Brunier, S.-E. Ouyahia, Numerical mixed convection heat transfer analysis in a ventilated irregular enclosure crossed by Cu-water nanofluid, *Arabian Journal of Science and Engineering* 42 (2017) 4575–4586.
46. J.C. Umavathi, A.J Chamkha, M.B. Mohite, Convective transport in a nanofluid-saturated porous layer with cross diffusion and variation of viscosity and conductivity, *Special Topics & Reviews in Porous Media: An International Journal* 6 (2015) 1–17.
47. J.C. Umavathi, M.B. Mohite, The onset of convection in a nanofluid saturated porous layer using Darcy model with cross diffusion, *Meccanica* 49 (2014) 1159–1175.
48. J.C. Umavathi, J.P. Kumar, Onset of convection in a porous medium layer saturated with an Oldroyd-B nanofluid, *Journal of Heat Transfer* 139(1) (2017) 012401.
49. R. Chowdhury, S. Parvin, M.A.H. Khan, Finite element analysis of double diffusive natural convection in a porous triangular enclosure filled with Al₂O₃ water nanofluid in presence of heat generation, *Heliyon* 2 (2016) e00140.
50. A.M. Aly, Z.A. Raizah, Double-diffusive natural convection in an enclosure filled with nanofluid using ISPH method, *Alexandria Engineering Journal* 55 (2016) 3037–3052.

51. J.C. Umavathi, M.A. Sheremet, O. Ojjela, G.J. Reddy, The onset of double-diffusive convection in a nanofluid saturated porous layer: Cross-diffusion effects, *European J. B/Fluids* 65 (2017) 70–87.
52. J.C. Umavathi, M.A. Sheremet, Onset of double-diffusive convection of a sparsely packed micropolar fluid in a porous medium layer saturated with a nanofluid, *Microfluidic Nanofluid* 21 (2017) 121–128.
53. A.V. Kuznetsov, D.A. Nield, Double-diffusive natural convective boundary layer flow of a nanofluid past a vertical plate, *Int. J. Thermal Sciences* 50 (2011) 712–717.
54. D.A. Nield, A.V. Kuznetsov, The Cheng–Minkowycz problem for the double diffusive natural convective boundary layer flow in a porous medium saturated by a nanofluid, *Int. J. Heat Mass Transfer* 54 (2011) 374–378.
55. A.G. Nnanna, Experimental model of temperature-driven nanofluid, *J. Heat Transfer* 129 (2006) 697–704.
56. H.F. Oztop, E. Abu-Nada, Numerical study of natural convection in partially heated rectangular enclosures filled with nanofluids, *Int. J. Heat Fluid Flow* 29 (2008) 1326–1336.
57. S.M. Aminossadati, B. Ghasemi, Natural convection cooling of a localized heat source at the bottom of a nanofluid-filled enclosure, *Eur. J. Mech. B. Fluids* 28 (2009) 630–640.
58. A.K. Santra, S. Sen, N. Chakraborty, Study of heat transfer characteristics of copper-water nanofluid in a differentially heated square cavity with different viscosity models, *J. Enhanced Heat Transfer* 15 (2008) 273–287.
59. M. Ghalambaz, M.A. Sheremet, S.A.M. Mehryan, F.M. Kashkooli, I. Pop, Local thermal non-equilibrium analysis of conjugate free convection within a porous enclosure occupied with Ag–MgO hybrid nanofluid, *Journal of Thermal Analysis and Calorimetry* 135 (2019) 1381–1398.
60. G. Diglio, C. Roselli, M. Sasso, J.C. Umavathi, Borehole heat exchanger with nanofluids as heat carrier, *Geothermic* 72 (2018) 112–123.
61. H.C. Brinkman, The viscosity of concentrated suspensions and solutions, *J. Chem. Phys.* 20 (1952) 571–581.
62. J. Maxwell, *Treatise A on Electricity and Magnetism*, 2nd Edition, Oxford University Press, Cambridge, UK, 1904.

- Double-diffusive free convection of nanofluid within a confined rectangular duct is investigated numerically.
- The fully developed flow is studied.
- The water-based nanoliquid including various nanoparticles with Soret and Dufour effects are assumed.
- The simulations are conducted using different nanoparticles, thermal Grashof number, solute Grashof number, solid volume fraction, Dufour number, Brinkman number, Prandtl number, and Soret number.

CRedit authorship contribution statement

J.C. Umavathi: Conceptualization, Methodology, Data curation, Writing - original draft, Writing - review & editing.

Bernardo Buonomo: Methodology, Writing - review & editing.

Oronzio Manca: Methodology, Writing - review & editing.

Mikhail A. Sheremet: Methodology, Writing - review & editing.

Journal Pre-proofs